Accepted Manuscript

Subdivision based mixed methods for isogeometric analysis of linear and nonlinear nearly incompressible materials

C. Kadapa, W.G. Dettmer, D. Perić

PII: S0045-7825(16)30095-0
DOI: http://dx.doi.org/10.1016/j.cma.2016.03.013
Reference: CMA 10884

To appear in: *Comput. Methods Appl. Mech. Engrg.*

Received date: 25 August 2015
Revised date: 7 March 2016
Accepted date: 9 March 2016

Please cite this article as: C. Kadapa, W.G. Dettmer, D. Perić, Subdivision based mixed methods for isogeometric analysis of linear and nonlinear nearly incompressible materials, *Comput. Methods Appl. Mech. Engrg.* (2016), http://dx.doi.org/10.1016/j.cma.2016.03.013

Subdivision based mixed methods for isogeometric analysis of linear and nonlinear nearly incompressible materials

C. Kadapa*, W.G. Dettmer, D. Perić

Zienkiewicz Centre for Computational Engineering, College of Engineering, Swansea University, Fabian Way, Swansea, SA1 8QQ, Wales, UK.

Abstract

This paper addresses the use of isogeometric analysis to solve solid mechanics problems involving nearly incompressible materials. The present work is focused on extension of two-field mixed variational formulations in both small and large strains to isogeometric analysis. *Inf-sup* stable displacement-pressure combinations for mixed formulations are developed based on the subdivision property of NURBS. Stability and convergence properties of the proposed displacement-pressure combinations are illustrated by computing numerical *inf-sup* constants and error norms. The performance of the proposed formulations is assessed by studying several benchmark examples involving nearly incompressible and incompressible elastic and elasto-plastic materials in both small and large strain regime.

Keywords: Isogeometric analysis; Mixed Galerkin formulations; Nearly incompressible materials; Subdivision stabilisation; *Inf-Sup* stability; Elasto-plastic material models.

1. Introduction

The isogeometric analysis (IGA) based on Non-Uniform Rational B-Spline (NURBS) introduced by Hughes *et al.* [14, 21] has proven to be an efficient alternative for the conventional Finite Element Method (FEM) as it offers great advantages in terms of accuracy. The principal reason is a higher order continuity of NURBS across element boundaries, which when coupled with k-refinement not only increases the continuity across element boundaries

*Corresponding author
Email address: c.kadapa@swansea.ac.uk (C. Kadapa)

but also reduces the total number of degrees of freedom (DOF). Isogeometric analysis has been extended to fluid-structure interaction [5], structural vibrations [15], phase-transition phenomenon [19] and other areas (see [14]). However, the research on the application of isogeometric analysis to the problems involving incompressible and nearly incompressible materials, especially *elasto-plastic* materials has received a limited attention, with only few articles published on the topic [16, 17, 23, 25, 27, 44].

In engineering analysis it is very common to perform simulations involving incompressible or nearly incompressible materials such as rubber, elastomers, and pressure-insensitive elasto-plastic materials. These material models often pose significant problems to the analyst, both in terms of accuracy and stability. When materials approach incompressible limit, the stiffening behaviour, often termed 'volumetric locking', is observed in load-displacement response. This is accompanied by a poor approximation of the pressure field, which often displays the so-called checkerboard pattern. To overcome this issue special elements and refined formulations and a combination of both are developed. Some of the widely used techniques to overcome *locking* are: reduced or selectively reduced integration [20], B-bar formulation for small-strain problems [20, 42, 47] and F-bar formulation for large-strain problems [29, 30], and hybrid or enhanced strain or stress elements [4, 31, 40, 41, 43].

As NURBS offer higher-order basis functions it is expected that pure displacement formulation based on NURBS should suffice in dealing with the incompressible and nearly incompressible material models. However, literature and our experience shows that NURBS still suffer from locking phenomenon and require additional measures to deal with incompressibility. Recently, Adam *et al.* [2] have studied selective and reduced integration schemes for NURBS based isogeometric analysis to deal with issue of *locking*. Elguedj *et al.* [16, 17] extended $\bar{\mathbf{B}}$ and $\bar{\mathbf{F}}$ projection methods to NURBS based isogeometric analysis. In our opinion, however, when $\bar{\mathbf{B}}$ and $\bar{\mathbf{F}}$ formulations are extended to higher order NURBS, the formulation and implementation becomes very complex, and loses appeal of the original methodologies that were applied to standard low-order polynomial interpolations. Furthermore, these methods require full matrix inversions on element level and also over an entire patch, thereby making them computationally expensive. Similar arguments can be made

about the macro-element projection technique used by Sangalli *et al.* [38] for nearly incompressible linear elastic materials. Mathisen *et al.* [27] and Taylor [44] extended the classical three-field Hu-Washizu mixed variational formulation to isogeometric analysis to deal with problems of incompressibility. However, the classical mixed formulation when applied to NURBS finite elements does not necessarily lead to the stable formulation. In addition, the three-field formulation increases the number of DOF substantially for higher order NURBS and as NURBS result in additional DOF because of their tensor product structure, the overall size of the problem increases exponentially, requiring substantially increased computational resources. Our experience with standard FE formulations also shows that three-field formulations are superfluous for most of the material models encountered in engineering simulations and that two-field formulations with displacement and pressure as independent variables provide sufficient accuracy and stability. In this work, therefore, we focus on the two-field mixed formulations for NURBS based isogeometric analysis in both the small and finite strain regimes.

The foremost problem associated with the mixed formulations is that they result in matrix system of equations with saddle-point nature. In order to obtain an accurate and stable solution the combination of approximating functions for displacement and pressure must satisfy the *inf-sup* or Ladyzhenskaya-Babuska-Brezzi (LBB) condition [9]. Following the work of Rüberg and Cirak [36, 37], in the present work we develop stable displacement-pressure NURBS combinations by exploiting the subdivison property of NURBS.

This paper is organised as follows. In Sections 2 and 3 we present the displacement and mixed variational formulations, respectively, in small and finite strain regimes. In Section 4 we give a brief introduction to NURBS. In Section 5 we discuss *inf-sup* stability criterion and construction of the stable displacement-pressure combinations, followed by the numerical evaluation of *inf-sup* constants. The accuracy and robustness of the proposed numerical schemes are demonstrated on a wide range of linear and nonlinear numerical examples in Sections 6 and 7. The paper is concluded with Section 8 with a summary of the present work and conclusions drawn from this work.

2. Small strain formulation

2.1. Governing equations

Consider a body Ω with boundary Γ embedded in three-dimensional Euclidian space $\mathbb{R}^3$. The boundary value problem of elasticity can be expressed as: Given $\mathbf{b}_0 : \Omega \to \mathbb{R}^3$, $\bar{\mathbf{g}} : \Gamma_D \to \mathbb{R}^3$ and $\bar{\mathbf{t}}_0 : \Gamma_N \to \mathbb{R}^3$, find $\mathbf{u} : \Omega \to \mathbb{R}^3$, such that:

$$\nabla \cdot \boldsymbol{\sigma} + \mathbf{b}_0 = \mathbf{0} \qquad \text{in} \quad \Omega, \tag{1}$$

$$\mathbf{u} = \bar{\mathbf{g}} \qquad \text{on} \quad \Gamma_D, \tag{2}$$

$$\boldsymbol{\sigma} \cdot \mathbf{n} = \bar{\mathbf{t}}_0 \qquad \text{in} \quad \Gamma_N, \tag{3}$$

where $\mathbf{u}$ is the displacement vector, $\boldsymbol{\sigma}$ is the Cauchy stress tensor, $\mathbf{b}_0$ is the body force, $\mathbf{n}$ is the unit outward normal on the boundary, Γ, of Ω, $\bar{\mathbf{g}}$ is the prescribed displacement on Γ_D and $\bar{\mathbf{t}}_0$ is the prescribed traction on Γ_N. Here, $\Gamma = \Gamma_D \cup \Gamma_N$. The stress tensor, $\boldsymbol{\sigma}$, is related to strain tensor, $\boldsymbol{\varepsilon}$, by the constitutive relation,

$$\boldsymbol{\sigma} = \mathcal{C}(\boldsymbol{\varepsilon}) \tag{4}$$

where,

$$\boldsymbol{\varepsilon} = \nabla^s \mathbf{u} = \frac{1}{2}\left(\nabla \mathbf{u} + \nabla \mathbf{u}^{\mathrm{T}}\right) \tag{5}$$

and $\mathcal{C}$ is, in general, a nonlinear mapping. The stress-strain relation (4) is linear for linear elastic material model and nonlinear in case of elasto-plastic material models.

In Galerkin formulations it is convenient to work with strain, stress and elasticity tensors by representing them in the matrix form. Strains and stresses transformed into matrix form are written as,

$$\boldsymbol{\varepsilon} = \left\{\varepsilon_{xx} \quad \varepsilon_{yy} \quad \varepsilon_{zz} \quad 2\varepsilon_{xy} \quad 2\varepsilon_{xz} \quad 2\varepsilon_{yz}\right\}^{\mathrm{T}} \tag{6}$$

$$\boldsymbol{\sigma} = \left\{\sigma_{xx} \quad \sigma_{yy} \quad \sigma_{zz} \quad \sigma_{xy} \quad \sigma_{xz} \quad \sigma_{yz}\right\}^{\mathrm{T}} \tag{7}$$

2.2. Displacement formulation

For a given displacement vector $\mathbf{u}$ and stored energy function $\mathrm{W}(\mathbf{u})$, the total energy functional is given by,

$$\Pi(\mathbf{u}) = \int_\Omega \mathrm{W}(\mathbf{u})\, \mathrm{d}\Omega \; - \; \Pi_{\text{ext}} \tag{8}$$

where Π_{ext} includes the effects of body forces, $\mathbf{b}_0$ and surface tractions, $\bar{\mathbf{t}}_0$, and is given as,

$$\Pi_{\text{ext}} = \int_\Omega \mathbf{u}^{\mathrm{T}} \mathbf{b}_0 \, \mathrm{d}\Omega + \int_\Gamma \mathbf{u}^{\mathrm{T}} \bar{\mathbf{t}}_0 \, \mathrm{d}\Gamma \tag{9}$$

For the system to be in equilibrium,

$$\delta\Pi = \int_\Omega \delta\boldsymbol{\varepsilon}^{\mathrm{T}} \boldsymbol{\sigma} \, \mathrm{d}\Omega - \delta\Pi_{\text{ext}} = \mathbf{0} \tag{10}$$

where,

$$\delta\Pi_{\text{ext}} = \int_\Omega \delta\mathbf{u}^{\mathrm{T}} \mathbf{b}_0 \, \mathrm{d}\Omega + \int_\Gamma \delta\mathbf{u}^{\mathrm{T}} \bar{\mathbf{t}}_0 \, \mathrm{d}\Gamma \tag{11}$$

By taking approximations for displacements as, $\mathbf{u} = \mathbf{N}_u \bar{\mathbf{u}}$, a Newton-Raphson iterative scheme leads to the following algebraic problem,

$$\mathbf{K}\, d\bar{\mathbf{u}} = -\mathbf{R}_u \tag{12}$$

where $\mathbf{N}_u$ is the matrix of shape functions, while $d\bar{\mathbf{u}}$ is the vector of increment in displacements. The stiffness matrix $\mathbf{K}$ and residual vector $\mathbf{R}_u$ are given as,

$$\mathbf{K} = \int_\Omega \mathbf{B}^{\mathrm{T}} \mathbf{D} \mathbf{B} \, \mathrm{d}\Omega \; ; \qquad \mathbf{R}_u = \int_\Omega \mathbf{B}^{\mathrm{T}} \boldsymbol{\sigma} \, \mathrm{d}\Omega - \mathbf{f} \tag{13a}$$

$$\text{with} \quad \mathbf{f} = \int_\Omega \mathbf{N}_u^{\mathrm{T}} \mathbf{b}_0 \, \mathrm{d}\Omega + \int_\Gamma \mathbf{N}_u^{\mathrm{T}} \bar{\mathbf{t}}_0 \, \mathrm{d}\Gamma \tag{13b}$$

where, $\mathbf{B}$ is the standard strain-displacement matrix for small strains, and $\mathbf{D}$ is termed the elastic moduli matrix.

For isotropic linear elasticity,

$$\mathbf{D} = 2\mu\, \mathbf{I}_0 + \lambda\, \mathbf{m}\mathbf{m}^{\mathrm{T}} \; ; \quad \boldsymbol{\sigma} = 2\mu\, \boldsymbol{\varepsilon} + \lambda\, (\nabla \cdot \mathbf{u})\, \mathbf{m} \tag{14}$$

where,

$$\mathbf{I}_0 = \mathrm{diag}\left[1 \quad 1 \quad 1 \quad \frac{1}{2} \quad \frac{1}{2} \quad \frac{1}{2}\right] \; ; \quad \mathbf{m}^{\mathrm{T}} = [1 \quad 1 \quad 1 \quad 0 \quad 0 \quad 0] \tag{15}$$

and μ and λ are the Lamé's constants. The derivation of elastic moduli matrix ($\mathbf{D}$) for elasto-plastic material models is much involved. For a detailed discussion on this topic we suggest the reader to refer to de Souza Neto *et al.* [28].

2.3. Two field mixed variational formulation

The main idea behind mixed formulations is to split the measure of deformation into deviatoric and volumetric components and replace the volumetric part by an improved value. In small strain formulation total strain, $\boldsymbol{\varepsilon}$, is the relevant measure of deformation and is additively decomposed into deviatoric and volumetric parts as,

$$\boldsymbol{\varepsilon} = \boldsymbol{\varepsilon}_{\text{dev}} + \boldsymbol{\varepsilon}_{\text{vol}} \tag{16}$$

with,

$$\boldsymbol{\varepsilon}_{\text{dev}} = \mathbf{I}_{\text{dev}}\boldsymbol{\varepsilon} \quad \text{and} \quad \boldsymbol{\varepsilon}_{\text{vol}} = \varepsilon_v \mathbf{m} \tag{17}$$

where,

$$\varepsilon_v = \mathbf{m}^{\mathrm{T}}\boldsymbol{\varepsilon}\ ; \quad \mathbf{I}_{\text{dev}} = \mathbf{I} - \frac{1}{3}\mathbf{m}\mathbf{m}^{\mathrm{T}} \tag{18}$$

in which $\mathbf{I}$ is the second-order identity tensor.

By defining hydrostatic pressure (also denoted the mean stress) as,

$$p = \frac{\sigma_x + \sigma_y + \sigma_z}{3} = \frac{\boldsymbol{\sigma}^{\mathrm{T}}\mathbf{m}}{3} \tag{19}$$

the total stress, $\boldsymbol{\sigma}$, can be additively split into deviatoric and volumetric parts,

$$\boldsymbol{\sigma} = \breve{\boldsymbol{\sigma}} = \boldsymbol{\sigma}_{\text{dev}} + p\,\mathbf{m} \tag{20}$$

Pressure, p, is related to the volumetric strain, ε_v, by the bulk modulus, κ, of the material, i.e.,

$$\varepsilon_v = \mathbf{m}^{\mathrm{T}}\boldsymbol{\varepsilon} = \frac{p}{\kappa} \tag{21}$$

By treating hydrostatic pressure, p, as an independent variable in addition to displacements, $\mathbf{u}$, we can formulate the problem using Eq. (10) and the weak form of Eq. (21) as,

$$\int_\Omega \delta\boldsymbol{\varepsilon}^{\mathrm{T}}\breve{\boldsymbol{\sigma}}\,\mathrm{d}\Omega = \int_\Omega \delta\mathbf{u}^{\mathrm{T}}\mathbf{b}_0\,\mathrm{d}\Omega + \int_\Gamma \delta\mathbf{u}^{\mathrm{T}}\bar{\mathbf{t}}_0\,\mathrm{d}\Gamma \tag{22a}$$

$$\int_\Omega \delta p\left[\mathbf{m}^{\mathrm{T}}\boldsymbol{\varepsilon} - \frac{p}{\kappa}\right]\,\mathrm{d}\Omega = 0 \tag{22b}$$

With $\mathbf{u} = \mathbf{N}_u\bar{\mathbf{u}}$ and $p = \mathbf{N}_p\bar{\mathbf{p}}$ as approximations for $\mathbf{u}$ and p and applying Newton-Raphson iterative scheme to solve Eq. (22) leads to the following algebraic problem,

$$\begin{bmatrix}\mathbf{K}_{uu} & \mathbf{K}_{up}\\ \mathbf{K}_{pu} & \mathbf{K}_{pp}\end{bmatrix}\begin{Bmatrix}d\bar{\mathbf{u}}\\ d\bar{\mathbf{p}}\end{Bmatrix} = -\begin{Bmatrix}\mathbf{R}_u\\ \mathbf{R}_p\end{Bmatrix} \tag{23}$$

where $d\bar{\mathbf{u}}$ and $d\bar{\mathbf{p}}$ are vectors of increments in displacements and pressure respectively. The corresponding stiffness matrices and residual vectors are given as,

$$\mathbf{K}_{uu} = \int_\Omega \mathbf{B}^{\mathrm{T}}\mathbf{D}_{\mathrm{dev}}\mathbf{B}\,\mathrm{d}\Omega\,; \quad \mathbf{K}_{up} = \int_\Omega \mathbf{B}^{\mathrm{T}}\mathbf{m}\mathbf{N}_p\,\mathrm{d}\Omega = \mathbf{K}_{pu}^{\mathrm{T}}\,; \quad \mathbf{K}_{pp} = -\int_\Omega \frac{1}{\kappa}\mathbf{N}_p^{\mathrm{T}}\mathbf{N}_p\,\mathrm{d}\Omega \tag{24}$$

$$\mathbf{R}_u = \int_\Omega \mathbf{B}^{\mathrm{T}}\breve{\boldsymbol{\sigma}}\,\mathrm{d}\Omega - \mathbf{f}\,; \qquad \mathbf{R}_p = \int_\Omega \mathbf{N}_p^{\mathrm{T}}\left[\mathbf{m}^{\mathrm{T}}\boldsymbol{\varepsilon} - \frac{p}{\kappa}\right]\,\mathrm{d}\Omega \tag{25}$$

and $\mathbf{f}$ is same as that given Eq. (13). Here, $\mathbf{D}_{\mathrm{dev}}$ is the deviatoric component of $\mathbf{D}$. For linear isotropic elastic material,

$$\mathbf{D}_{\mathrm{dev}} = 2\mu\left(\mathbf{I}_0 - \frac{1}{3}\mathbf{m}\,\mathbf{m}^{\mathrm{T}}\right) \tag{26}$$

3. Finite strain formulation

3.1. Governing equations

Let Ω be the reference configuration of a body and ω_ϕ be its deformed configuration. Let $\boldsymbol{\phi} : \Omega \to \omega_\phi$ be a mapping that takes a point $\mathbf{X} \in \Omega$ to a point $\mathbf{x} \in \omega_\phi$. The displacement of a point from its initial position $\mathbf{X}$ to its current configuration $\mathbf{x}$ is given by

$$\mathbf{u}(\mathbf{X}) = \boldsymbol{\phi}(\mathbf{X}) - \mathbf{X} = \mathbf{x} - \mathbf{X} \tag{27}$$

The deformation gradient, $\mathbf{F}$, the right Cauchy-Green deformation tensor, $\mathbf{C}$, the left Cauchy-Green deformation tensor, $\mathbf{b}$, and the Green-Lagrange strain tensor, $\mathbf{E}$, are defined as,

$$\mathbf{F} = \frac{\partial \mathbf{x}}{\partial \mathbf{X}} = \mathbf{I} + \frac{\partial \mathbf{u}}{\partial \mathbf{X}}; \qquad \mathbf{C} = \mathbf{F}^{\mathrm{T}}\mathbf{F}; \qquad \mathbf{b} = \mathbf{F}\mathbf{F}^{\mathrm{T}}; \qquad \mathbf{E} = \frac{1}{2}\left(\mathbf{C} - \mathbf{I}\right) \tag{28}$$

For a given free-energy function $W(\mathbf{C})$, the second Piola-Kirchhoff stress tensor, $\mathbf{S}$, is defined as,

$$\mathbf{S} = 2\frac{\partial W}{\partial \mathbf{C}} = \frac{\partial W}{\partial \mathbf{E}} \tag{29}$$

The boundary value problem of elasticity in large strain regime for a body with reference configuration Ω can be stated as:
Given $\mathbf{b}_0 : \Omega \to \mathbb{R}^3$, $\bar{\mathbf{g}} : \Gamma_D \to \mathbb{R}^3$ and $\bar{\mathbf{t}}_0 : \Gamma_N \to \mathbb{R}^3$, find $\mathbf{u} : \Omega \to \mathbb{R}^3$, such that:

$$\nabla_{\mathrm{X}} \cdot \mathbf{P} + \mathbf{b}_0 = \mathbf{0} \qquad \text{in} \quad \Omega, \tag{30}$$

$$\mathbf{u} = \bar{\mathbf{g}} \qquad \text{on} \quad \Gamma_D, \tag{31}$$

$$\mathbf{P} \cdot \mathbf{N} = \bar{\mathbf{t}}_0 \qquad \text{in} \quad \Gamma_N, \tag{32}$$

where $\mathbf{b}_0$ is the body force per unit undeformed volume, $\mathbf{N}$ is the unit outward normal on the boundary, Γ, of Ω, $\bar{\mathbf{g}}$ is the prescribed displacement on Γ_D, $\bar{\mathbf{t}}_0$ is the prescribed traction per unit area on Γ_N, with $\Gamma = \Gamma_D \cup \Gamma_N$, and $\mathbf{P}$ is the first Piola-Kirchhoff stress tensor, defined as,

$$\mathbf{P} = \mathbf{F}\,\mathbf{S} \tag{33}$$

3.2. Displacement formulation

For a given stored energy function, W, the total energy functional, in the reference configuration, Ω, is given by,

$$\Pi(\mathbf{u}) = \int_{\Omega} W(\mathbf{C})\, \mathrm{d}\Omega \; - \; \Pi_{\text{ext}} \tag{34}$$

where, Π_{ext} is same as that given Eq. (9).

By taking approximations for displacements as, $\mathbf{u} = \mathbf{N}_u \bar{\mathbf{u}}$, and applying the Newton-Raphson scheme to the nonlinear system of equations resulting from the equilibrium leads to the following algebraic problem,

$$\mathbf{K}\, d\bar{\mathbf{u}} = -\mathbf{R}_u \tag{35}$$

where,

$$\mathbf{R}_u = \int_\omega \mathbf{B}^{\mathrm{T}} \boldsymbol{\sigma} \, \mathrm{d}\omega - \mathbf{f} \tag{36}$$

Assuming that loads are independent of the configuration of the domain, the stiffness matrix $\mathbf{K}$ is given by,

$$\mathbf{K} = \mathbf{K}_M + \mathbf{K}_G \tag{37}$$

where, material stiffness matrix $\mathbf{K}_M$ and geometric stiffness matrix $\mathbf{K}_G$ are given as,

$$\mathbf{K}_M = \int_\omega \mathbf{B}^{\mathrm{T}} \mathbf{D} \mathbf{B} \, \mathrm{d}\omega \quad \text{and} \quad \mathbf{K}_G = \int_\omega (\mathbf{N}_{a,i} \boldsymbol{\sigma}_{ij} \mathbf{N}_{b,j}) \, \mathbf{I} \, \mathrm{d}\omega \tag{38}$$

and $\mathbf{f}$ is same as that given in small strain formulation in Eq. (13b). Here, the elastic modulii matrix $\mathbf{D}$ depends upon the material model considered in the analysis. For the comprehensive details on the derivation of $\mathbf{D}$ from the energy function of a material model and for the detailed description of the formulations used in this paper the reader is referred to Zienkiewicz and Taylor [47] and Bonet and Wood [6].

3.3. Two field mixed variational formulation

The mixed formulation in the finite strain regime is based on the multiplicative split of the deformation gradient, $\mathbf{F}$, into deviatoric and volumetric components such that,

$$\mathbf{F} = \mathbf{F}_{\mathrm{vol}} \mathbf{F}_{\mathrm{dev}} \tag{39}$$

where,

$$\mathbf{F}_{\mathrm{vol}} = J^{1/3} \mathbf{I}, \quad \mathbf{F}_{\mathrm{dev}} = J^{-1/3} \mathbf{F} \quad \text{with} \quad J = \det \mathbf{F} \tag{40}$$

Using (40) the modified right Cauchy-Green tensor, $\bar{\mathbf{C}}$, and the modified left Cauchy-Green tensor, $\bar{\mathbf{b}}$, are defined as,

$$\bar{\mathbf{C}} = \mathbf{F}_{\mathrm{dev}}^{\mathrm{T}} \, \mathbf{F}_{\mathrm{dev}} \quad \text{and} \quad \bar{\mathbf{b}} = \mathbf{F}_{\mathrm{dev}} \, \mathbf{F}_{\mathrm{dev}}^{\mathrm{T}} \tag{41}$$

Considering displacements, $\mathbf{u}$ and pressures, p, as independent variables, the modified potential energy functional can be written as,

$$\Pi(\mathbf{u}, p) = \int_\Omega \left[W(\mathbf{C}) + p(J-1) - \frac{1}{2\kappa} p^2 \right] \, \mathrm{d}\Omega - \Pi_{\mathrm{ext}} \tag{42}$$

For all of the material models considered in the examples presented, W can be represented as the additive decomposition of deviatoric and volumetric parts, as,

$$W(\mathbf{C}) = W^{\text{dev}}(J, \bar{\mathbf{C}}) + W^{\text{vol}}(J) \tag{43}$$

Similar to small-strain formulation, by taking approximations for variables $\mathbf{u}$ and p as $\mathbf{u} = \mathbf{N}_u \bar{\mathbf{u}}$ and $p = \mathbf{N}_p \bar{\mathbf{p}}$ and after applying Newton-Raphson iterative scheme an algebraic problem is obtained given as,

$$\begin{bmatrix} \mathbf{K}_{uu} & \mathbf{K}_{up} \\ \mathbf{K}_{pu} & \mathbf{K}_{pp} \end{bmatrix} \begin{Bmatrix} d\bar{\mathbf{u}} \\ d\bar{\mathbf{p}} \end{Bmatrix} = - \begin{Bmatrix} \mathbf{R}_u \\ \mathbf{R}_p \end{Bmatrix} \tag{44}$$

where,

$$\mathbf{K}_{uu} = \int_\Omega \mathbf{B}^{\mathrm{T}} \bar{\mathbf{D}}_{11} \mathbf{B} \; J \; \mathrm{d}\Omega \; + \; \mathbf{K}_G \; ; \quad \mathbf{K}_{up} = \int_\Omega \mathbf{B}^{\mathrm{T}} \mathbf{m} \mathbf{N}_p \; J \; \mathrm{d}\Omega = \mathbf{K}_{pu}^{\mathrm{T}} \tag{45}$$

$$\mathbf{R}_u = \int_\Omega \mathbf{B}^{\mathrm{T}} \breve{\boldsymbol{\sigma}} J \; \mathrm{d}\Omega - \mathbf{f} \; ; \quad \mathbf{R}_p = \int_\Omega \mathbf{N}_p^{\mathrm{T}} \left(J - 1 - \frac{p}{\kappa} \right) \; \mathrm{d}\Omega \tag{46}$$

with,

$$\bar{\mathbf{D}}_{11} = \mathbf{I}_{\text{dev}} \mathbf{D} \mathbf{I}_{\text{dev}} \; - \; \frac{2}{3} \left(\mathbf{m} \boldsymbol{\sigma}_{\text{dev}}^{\mathrm{T}} + \boldsymbol{\sigma}_{\text{dev}} \mathbf{m}^{\mathrm{T}} \right) \; + \; 2 \left(\bar{p} - p \right) \mathbf{I}_0 \; - \; \left(\frac{2}{3} \bar{p} - p \right) \mathbf{m} \mathbf{m}^{\mathrm{T}} \tag{47}$$

$$\breve{\boldsymbol{\sigma}} = \boldsymbol{\sigma} + \mathbf{m}(p - \bar{p}) \quad \text{and} \quad \bar{p} = \frac{1}{3} \mathbf{m}^{\mathrm{T}} \boldsymbol{\sigma} \tag{48}$$

4. NURBS and Isogeometric Analysis

4.1. Introduction to NURBS

NURBS are the standard tools to model geometries in Computer Aided Design (CAD) industry. NURBS are a generalization of B-Splines which are composed of linear combinations of B-Spline basis functions.

Given a knot vector $\boldsymbol{\Xi} = \{\xi_0, \ldots, \xi_{n+a+1}\}$ and degree of polynomial a, B-Spline basis functions are defined as follows:

For $a = 0$, (piece-wise constants),

$$N_{i,0}(\xi) = \begin{cases} 1 & \text{if } \xi_i \leq \xi \leq \xi_{i+1} \\ 0 & \text{otherwise} \end{cases}$$

and for $a \geq 1$,

$$N_{i,a}(\xi) = \frac{\xi - \xi_i}{\xi_{i+a} - \xi_i} N_{i,a-1}(\xi) + \frac{\xi_{i+a+1} - \xi}{\xi_{i+a+1} - \xi_{i+1}} N_{i+1,a-1}(\xi) \tag{49}$$

NURBS geometries are represented as a linear combination of B-Spline basis functions along with a set of control points. A NURBS curve of degree a is defined as,

$$\mathbf{X}(\xi) = \sum_{i=0}^{n} N_{i,a}(\xi) \mathbf{P}_i^w \quad \text{for} \quad 0 \leq \xi \leq 1 \tag{50}$$

where $\{\mathbf{P}_i^w\}$, $i = 0, 1, ..., n$ is the control polygon and $N_{i,a}$ is a B-Spline basis function of degree a defined on a knot vector $\boldsymbol{\Xi}$. Control points are represented in homogeneous coordinates as they offer many advantages in mathematical treatment as well as programming.

NURBS objects in higher-dimensions are created as tensor products of univariate NURBS. A NURBS surface of degree a in ξ direction and degree b in η direction is defined as,

$$\mathbf{X}(\xi, \eta) = \sum_{i=0}^{n} \sum_{j=0}^{m} N_{i,a}(\xi) M_{j,b}(\eta) \mathbf{P}_{i,j}^w \quad \text{for} \quad 0 \leq \xi, \eta \leq 1 \tag{51}$$

where $\{\mathbf{P}_{i,j}^w\}$, $i = 0, 1, ..., n$, $j = 0, 1, ..., m$ is the control net and $N_{i,a}(\xi)$ and $M_{j,b}(\eta)$ are the B-Spline basis functions, respectively, on knot vectors $\boldsymbol{\Xi}_1 = \{\xi_0, \ldots, \xi_{n+a+1}\}$, and $\boldsymbol{\Xi}_2 = \{\eta_0, \ldots, \eta_{m+b+1}\}$.

Similarly, a NURBS solid is defined as,

$$\mathbf{X}(\xi, \eta, \zeta) = \sum_{i=0}^{n} \sum_{j=0}^{m} \sum_{k=0}^{l} N_{i,a}(\xi) M_{j,b}(\eta) L_{k,c}(\zeta) \mathbf{P}_{i,j,k}^w \quad \text{for} \quad 0 \leq \xi, \eta, \zeta \leq 1 \tag{52}$$

for a given a control net $\{\mathbf{P}_{i,j,k}^w\}$, $i = 0, 1, ..., n$, $j = 0, 1, ..., m$, $k = 0, 1, ..., l$ and knot vectors $\boldsymbol{\Xi}_1 = \{\xi_0, \ldots, \xi_{n+a+1}\}$, $\boldsymbol{\Xi}_2 = \{\eta_0, \ldots, \eta_{m+b+1}\}$ and $\boldsymbol{\Xi}_3 = \{\zeta_0, \ldots, \zeta_{l+c+1}\}$. The reader is suggested to refer to [14, 18, 32, 35] for further details on this topic.

4.2. NURBS spaces for isogeometric analysis

The basic idea of isogeometric analysis is to use the same basis functions used to represent the geometry as the approximating functions for the field variables. Using the NURBS basis functions as approximating functions the field variables can be approximated as,

$$\mathbf{u} = \sum_{\alpha=0} \mathbf{N}_\alpha(\boldsymbol{\xi})\, \bar{\mathbf{u}}_\alpha; \quad p = \sum_{\alpha=0} \mathbf{N}_\alpha(\boldsymbol{\xi})\, \bar{\mathbf{p}}_\alpha \tag{53}$$

where $\boldsymbol{\xi} = \{\xi, \eta, \zeta\}$ are the parametric coordinates, $\bar{\mathbf{u}}_\alpha$ and $\bar{\mathbf{p}}_\alpha$ are the control variables which similar to nodal values in standard finite element method and $\mathbf{N}(\boldsymbol{\xi})$ are the multivariate basis functions determined from the knot vectors and degrees of polynomial in each parametric direction. $\mathbf{N}(\boldsymbol{\xi})$ are computed as tensor products of univariate basis functions, as given by

$$\mathbf{N}(\boldsymbol{\xi}) = \mathbf{M}(\xi) \otimes \mathbf{M}(\eta) \qquad \text{in} \quad 2\text{D} \tag{54}$$

$$\mathbf{N}(\boldsymbol{\xi}) = \mathbf{M}(\xi) \otimes \mathbf{M}(\eta) \otimes \mathbf{M}(\zeta) \qquad \text{in} \quad 3\text{D} \tag{55}$$

where $\mathbf{M}(\xi)$, $\mathbf{M}(\eta)$ and $\mathbf{M}(\zeta)$ are the univariate basis functions in ξ, η, and ζ directions respectively. Note that $\mathbf{N}(\boldsymbol{\xi})$ is normally stored in the form of a vector.

As a convention to represent NURBS approximation spaces of different orders, let us denote Q_a as approximations of order a. The continuity of Q_a elements within a patch can be of any order k which varies from 0 to $(a-1)$, depending upon the multiplicity of the internal knots. All the knot vectors are assumed to be open, so a patch constructed on such knot vectors would be interpolatory at the ends and hence in case of problems modeled with multiple patches, only $\mathcal{C}^0$ continuity is achieved across the patch interfaces. For further details on this topic the reader is referred to Cottrell *et al.* [14].

5. Mixed formulation and the *inf-sup* condition

The saddle-point nature of matrix system obtained with the mixed Galerkin formulations, Eqs. (23) and (44), pose difficulties in obtaining stable numerical solutions. The combination of approximation spaces for displacement and pressure has to be chosen in such a way that it satisfies the *inf-sup* or LBB condition and failing to do so results in spurious oscillations in pressure. The standard practice with the Lagrange finite elements is to choose basis functions for pressure to be one order lower than those for the displacement, the Taylor-Hood element being a classical example [8, 9]. Several researchers [16, 22, 24, 27, 44] extended this strategy to mixed formulations for IGA for solid mechanics. However, [11, 36] and our experience shows that NURBS combination Q_a/Q_{a-1} (Q_a for displacement and Q_{a-1} for pressure with the same knot discretisation) is unstable with respect to LBB condition. To

overcome this issue, Bressan and Sangalli [7] developed several *inf-sup* stable displacement-pressure combinations for NURBS based IGA using macro-element projection technique and employed it for the analysis of linear nearly incompressible elasticity in [3, 38]. However, as such projection techniques involve element-level matrix inversions, we do not find such techniques to be computationally appealing when used in the context of higher-order elements. Moreover, as we use the mixed formulations directly, i.e., without condensation, we have difficulty in justifying the use of discontinuous spaces for pressure discretisation, as the use of such element-level discontinuous spaces seems to be in contradiction with the idea behind NURBS based IGA, namely, use of higher-order shape functions with high continuity across element boundaries. Hence, in the present work we develop *inf-sup* stable displacement-pressure combinations for NURBS based IGA based on subdivision properties of NURBS inspired by the stable velocity-pressure combinations proposed by Rüberg and Cirak [36].

5.1. Subdivision properties of B-Splines

One of the interesting properties of B-Spline functions is their two-scale relation. According to this property B-Spline basis functions on a knot-vector with knot-spacing h can be represented as a linear combinations of B-Spline basis functions on a knot-vector with knot-spacing $h/2$ as illustrated in Fig. 1. The coarse basis functions in Fig. 1(a) and Fig. 1(b) can be presented as a linear combinations of fine basis functions in Fig. 1(c) and Fig. 1(d), respectively.

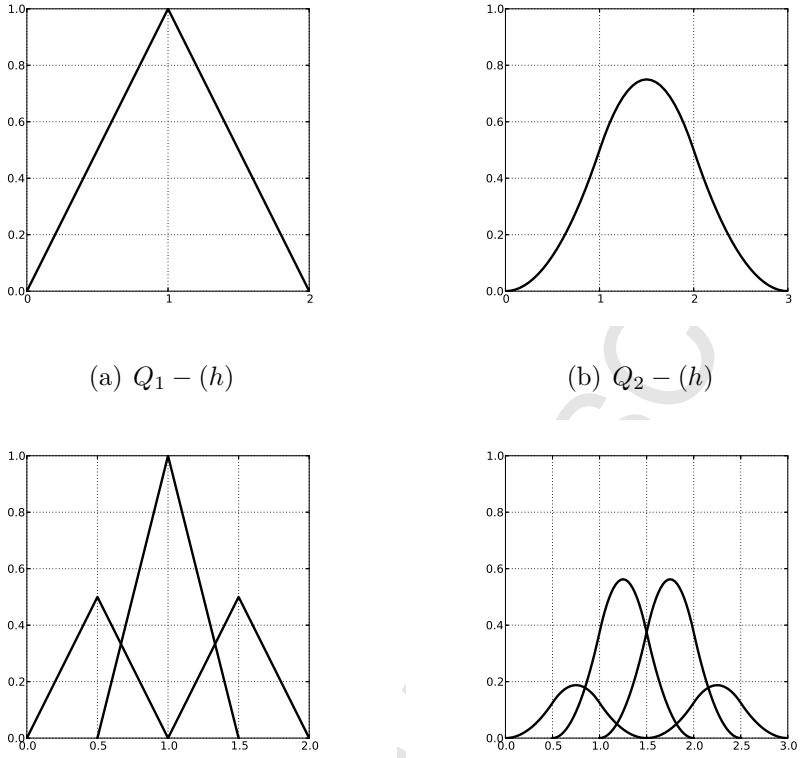

(a) $Q_1 - (h)$ (b) $Q_2 - (h)$

(c) $Q_1 - (h/2)$ (d) $Q_2 - (h/2)$

Figure 1: Subdivision property of B-Spline basis functions in 1D.

The two-scale relation can be written as,

$$\mathbf{N}_k = \mathbf{S}\,\mathbf{N}_{k+1} \tag{56}$$

where, $\mathbf{N}_k$ and $\mathbf{N}_{k+1}$ are the basis functions, respectively, at levels k and $k+1$, and $\mathbf{S}$ is the subdivision matrix. In one-dimension, the subdivision matrices for linear and quadratic B-Splines are,

$$\mathbf{S}_{Q_1} = \begin{bmatrix} \frac{1}{2} & 1 & \frac{1}{2} \end{bmatrix} \; ; \quad \mathbf{S}_{Q_2} = \begin{bmatrix} \frac{1}{4} & \frac{3}{4} & \frac{3}{4} & \frac{1}{4} \end{bmatrix} \tag{57}$$

5.2. Subdivision properties of NURBS

Similarly, NURBS basis functions defined on a knot-spacing h can be represented as a linear combination of those defined on a knot-spacing $h/2$. Each of the NURBS basis functions in Figs. 2(a) and 2(b) can be represented as a linear combination of NURBS basis

functions in Figs. 2(c) and 2(d), respectively. The entries of the subdivision matrix **S** in Eq. (56) can be computed by following the definitions of NURBS basis functions.

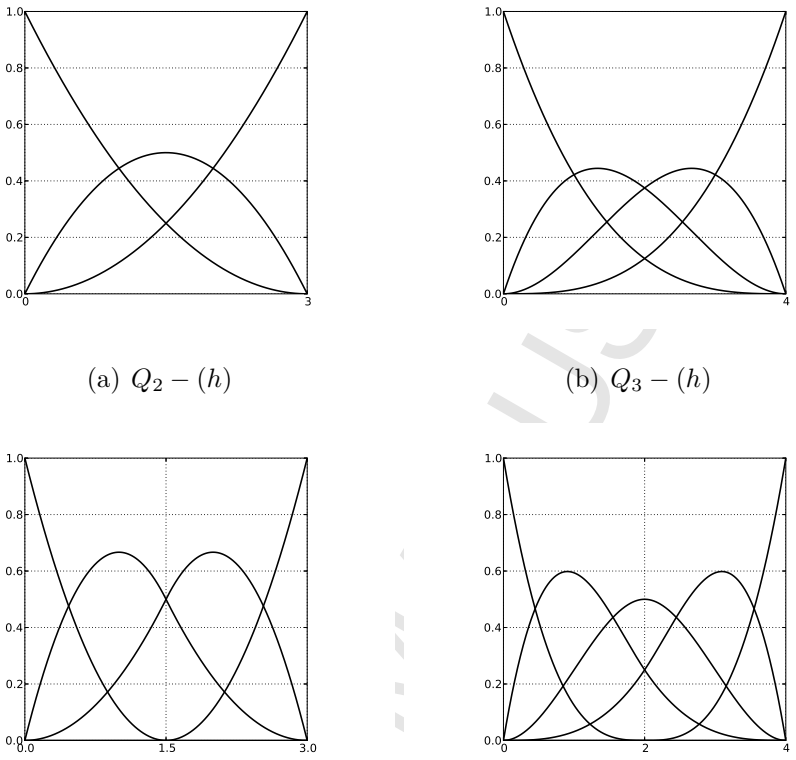

(a) $Q_2 - (h)$ (b) $Q_3 - (h)$

(c) $Q_2 - (h/2)$ (d) $Q_3 - (h/2)$

Figure 2: Subdivision property of NURBS basis functions in 1D.

5.3. NURBS spaces for mixed formulation

Based on the subdivision properties, we develop displacement-pressure combinations — denoted as Q_a/Q_b-SD — in which Q_a NURBS discretisation for displacement is combined with Q_b NURBS discretisation for pressure with the element knot-span for pressure being double that of displacement. In other words one pressure element in n- spatial dimensions spans 2^n displacement elements, as illustrated in Fig. 3. Figures on the left are for displacement discretisation and those on the right are for the pressure discretisation.

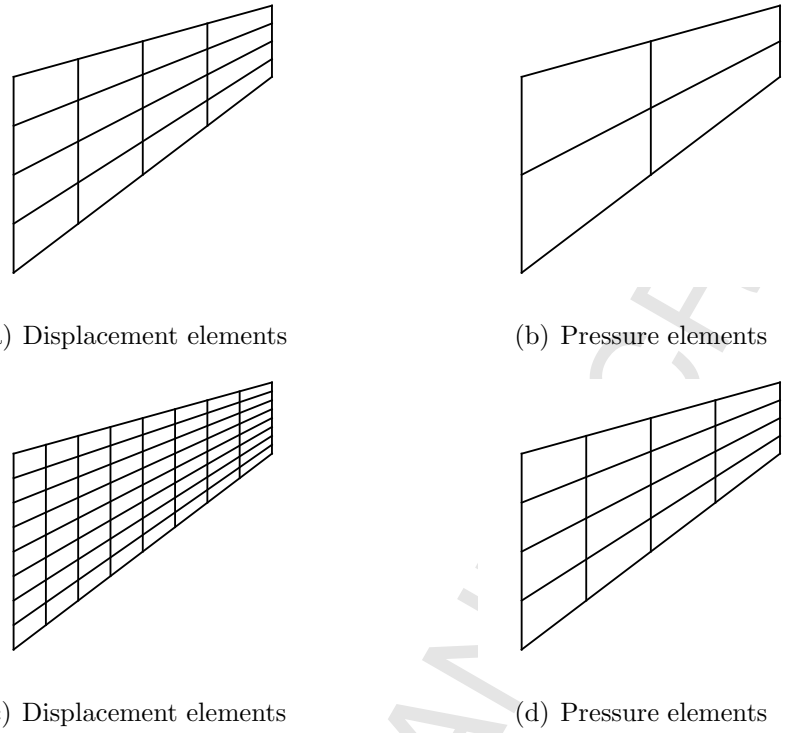

(a) Displacement elements (b) Pressure elements

(c) Displacement elements (d) Pressure elements

Figure 3: Subdivision based discretisations for displacement and pressure.

5.4. Numerical inf-sup test

Recall that for a given displacement discretisation $\mathbf{u}_h \in \mathcal{U}_h$ and pressure discretisation $p_h \in \mathcal{P}_h$ the *inf-sup* condition is given by the inequality [9]

$$\inf_{p_h \in \mathcal{P}_h} \sup_{\mathbf{u}_h \in \mathcal{U}_h} \frac{\int_\Omega p_h \mathrm{div}\mathbf{u}_h \, \mathrm{d}\Omega}{\|\mathbf{u}_h\| \|p_h\|} \geq \beta_h > 0 \tag{58}$$

The displacement and pressure discretisation combination has to satisfy the above inequality in order to obtain stable pressure solutions using the mixed formulations. Obtaining analytical proof of *inf-sup* condition in a general setting is quite challenging and to our knowledge no such proofs are available yet for NURBS based discretisations. Even many of the widely used displacement-pressure combinations (and velocity-pressure combinations in fluid mechanics) in engineering practice have no analytical proofs yet. Towards addressing this issue Chapelle and Bathe [12] proposed a numerical test. The test involves the calculation of β_h values over a sequence of mesh refinements. If the value of β_h does not decrease towards zero as the mesh is refined then the test is passed and displacement-pressure combination

is considered to be stable. Otherwise, the displacement-pressure combination is considered unstable.

The value of β_h is computed as the square-root of the smallest non-zero eigenvalue (λ_h) of the following generalised eigenvalue system

$$\mathbf{K}_{pu}\mathbf{G}_h^{-1}\mathbf{K}_{up}\bar{\mathbf{p}} = \lambda_h\,\mathbf{M}_h\bar{\mathbf{p}} \tag{59}$$

where,

$$\mathbf{G}_h = \int_\Omega \nabla\mathbf{N}_u^T : \nabla\mathbf{N}_u \,\mathrm{d}\Omega \tag{60}$$

$$\mathbf{M}_h = \int_\Omega \mathbf{N}_p^T\mathbf{N}_p \,\mathrm{d}\Omega \tag{61}$$

In this work we demonstrate the stability characteristics of different combinations of NURBS spaces by computing numerically the *inf-sup* constants for Cook's membrane and a thick-walled cylinder. Two different examples are chosen in order to demonstrate the robustness of the proposed spaces for geometries that are represented by non-rational as well as rational polynomials.

5.4.1. Inf-sup test - Cook's membrane

The standard Cook's membrane is composed of a nearly incompressible elastic material and loaded by edge load under plane strain conditions. Geometry and boundary conditions of the problem are shown in Fig. 4. The initial mesh consists of a single element with linear NURBS and it is k-refined to obtain the meshes shown in Fig. 5. Numerical values of *inf-sup* constants computed for the different meshes for different orders of NURBS basis functions are presented in log-log scale in Fig. 6. It is evident from these graphs that all the displacement-pressure combinations with subdivision, Q_a/Q_a-SD and Q_a/Q_{a-1}-SD, are *inf-sup* stable and those without subdivision, Q_a/Q_a and Q_a/Q_{a-1}, are not.

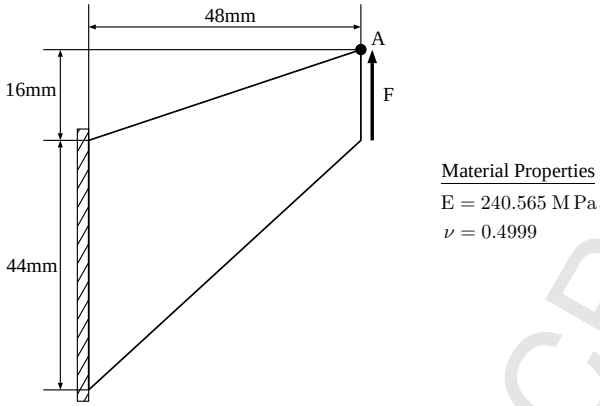

Figure 4: Cook's membrane: geometry, loading, boundary conditions and material properties.

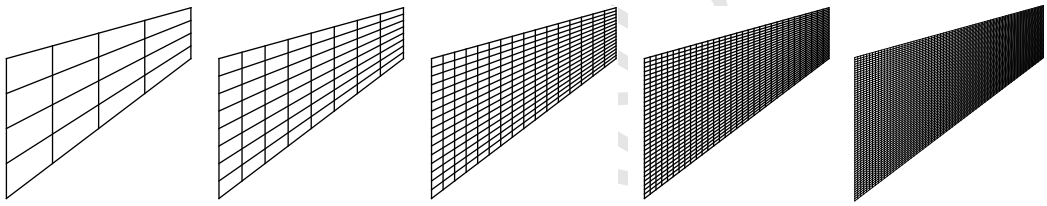

Figure 5: Cook's membrane: meshes used for the analysis.

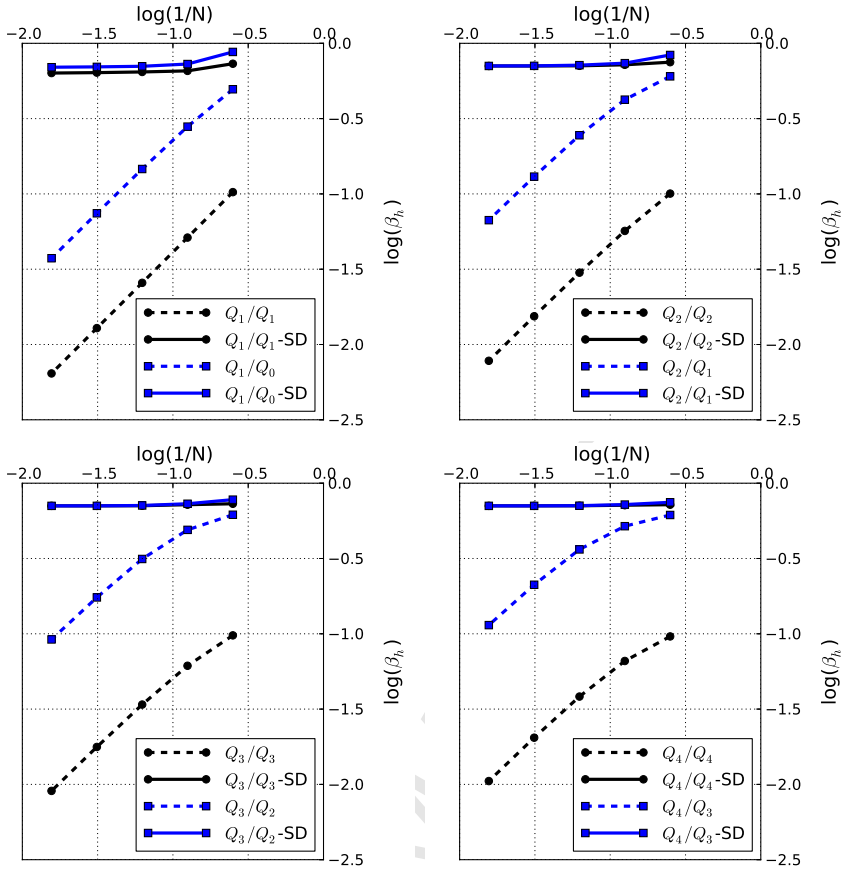

Figure 6: Cook's membrane: numerical *inf-sup* constants versus number of elements per side (N) for different orders of NURBS basis functions.

5.4.2. Inf-sup test - thick-walled cylinder

The geometry and boundary conditions of the problem are shown in Figure 7. As the geometry includes portions of the circle it can be represented exactly with quadratic and higher-order NURBS. An initial mesh of one element with Q_2 NURBS is k-refined to generate successively refined meshes shown in Fig. 8. The computed values of *inf-sup* constants, shown in Fig. 9, follow the same trend as that observed in Cook's membrane example: for a particular order of NURBS numerical *inf-sup* value remains constant with mesh refinement subdivision stabilised displacement-pressure combinations and it approaches zero for those without subdivision. In other words, the displacement-pressure combinations Q_a/Q_a-SD and Q_a/Q_{a-1}-SD are *inf-sup* stable and the combinations Q_a/Q_a and Q_a/Q_{a-1} are not.

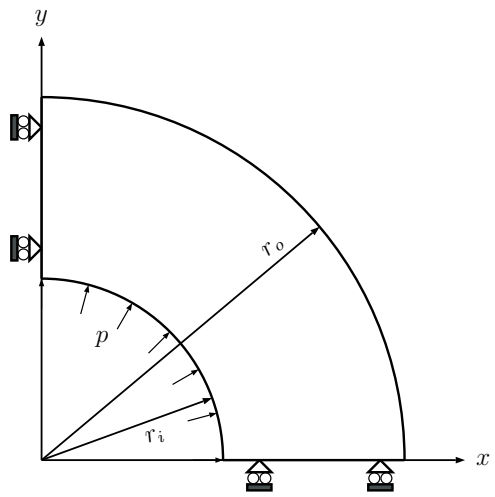

Inner radius (r_i) = 100 mm

Outer radius (r_o) = 200 mm

Young's modulus (E) = 210 GPa

Internal pressure (p) = 0.1 GPa

Figure 7: Thick-walled cylinder: geometry and boundary conditions.

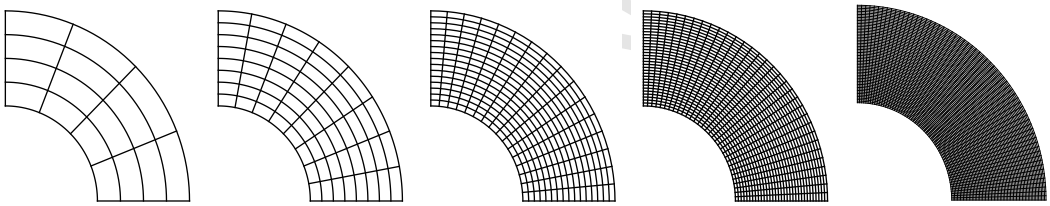

Figure 8: Thick-walled cylinder: meshes used for the analysis.

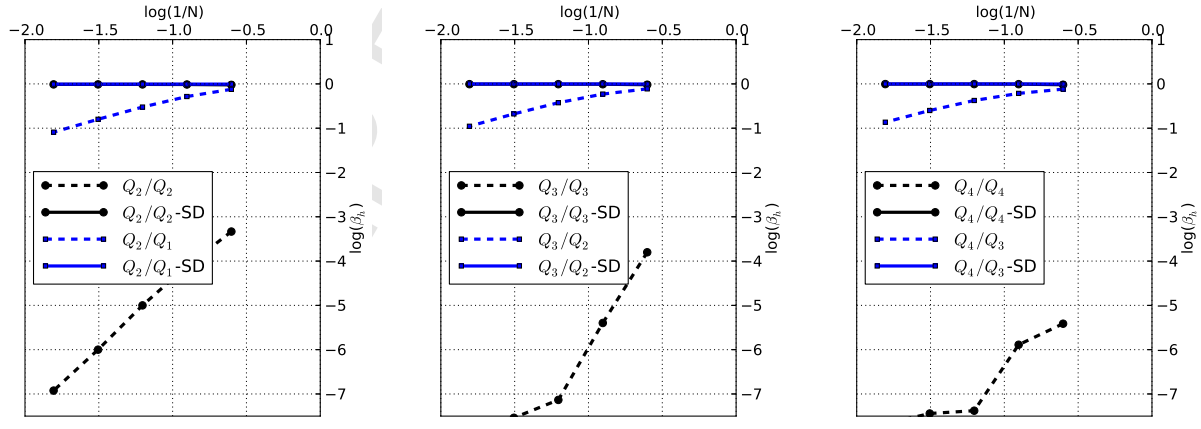

Figure 9: Thick-walled cylinder: numerical *inf-sup* constants versus the number of elements per side (N) for different orders of NURBS basis functions.

6. Numerical examples - small strain

In all of the examples considered to demonstrate the performance of the proposed formulations, an initial coarse geometry is defined and then *k-refinement* of isogeometric analysis as introduced by Cottrell *et al.* [14, 21], is followed to achieve the desired refinement. According to k-refinement, order of the polynomial is increased first and then required knot insertions are performed. We note that this new type of refinement procedure has no analogous in the standard FEM. The refinement has the advantage that it reduces the number of control points and also increases the continuity across the newly inserted knots (element boundaries).

In the present work we have used a direct solver (PARDISO [1]) to solve the resulting matrix system.

6.1. Thick-walled cylinder subjected to internal pressure

The first example is the analysis of thick-walled cylinder subjected to internal pressure. Plane strain condition is assumed because of the geometry of the problem and only quarter portion of the cylinder is modelled, as shown in Figure 7, due to the symmetry of geometry and loading conditions. For this problem analytical solutions for displacement and stress are available [45]. Analytical expressions for radial displacement (d_r), radial stress (σ_{rr}), hoop stress ($\sigma_{\theta\theta}$) and shear stress ($\tau_{r\theta}$) are given as:

$$d_r = \frac{p\, r_i^2}{(r_o^2 - r_i^2)\, E} \left[(1 - \nu - 2\nu^2)\, r + (1 + \nu)\, \frac{r_o^2}{r} \right] \tag{62}$$

$$\sigma_{rr} = \frac{p\, r_i^2}{r_o^2 - r_i^2} \left[1 - \frac{r_o^2}{r^2} \right] \tag{63}$$

$$\sigma_{\theta\theta} = \frac{p\, r_i^2}{r_o^2 - r_i^2} \left[1 + \frac{r_o^2}{r^2} \right] \tag{64}$$

$$\tau_{r\theta} = 0 \tag{65}$$

where r is the radius at an arbitrary point in the domain. These analytical solutions are used to compute error norms in order to assess the convergence properties of the proposed numerical scheme.

The convergence studies are performed on successively refined meshes for two different values of Poisson's ratio, $\nu = 0.4$ and $\nu = 0.49999$, in order to demonstrate the robustness of the proposed displacement-pressure combinations in both the compressible and nearly incompressible regimes. Convergence graphs of L^2-norm of absolute error in displacement, L^2-norm of absolute error in stress and energy norm error are shown in Fig. 10 and Fig. 11, respectively, for $\nu = 0.4$ and $\nu = 0.49999$. The mesh parameter h is considered to be the maximum of all element diagonal lengths in the physical domain. These graphs indicate that optimal convergence rates are obtained for both the displacement-pressure combinations, Q_a/Q_a-SD and Q_a/Q_{a-1}-SD. Even though the pure displacement formulation results in better than optimal convergence rates in displacement for $\nu = 0.49999$, the stresses obtained are of a very poor quality, as can be observed from the graph Fig. 6.1 and the contour plots Fig. 12(a) and Fig. 13(a). The two-field mixed formulation with the proposed displacement-pressure combinations results in smooth stress field of substantially reduced errors along with maintaining optimal convergence. The contour plots of radial and hoop stresses shown, respectively, in Fig. 12 and Fig. 13, illustrate that the proposed displacement-pressure combinations produce stress fields without any spurious oscillations.

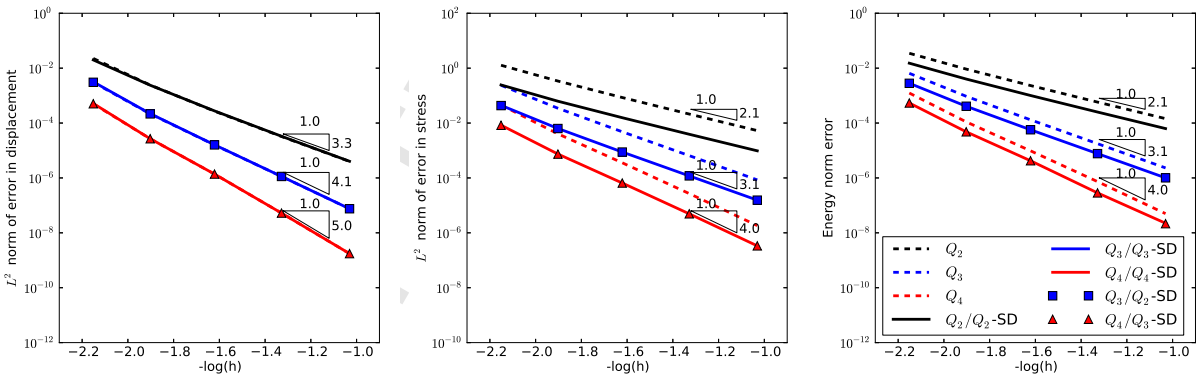

Figure 10: Thick-walled cylinder: error norms for $\nu = 0.4$.

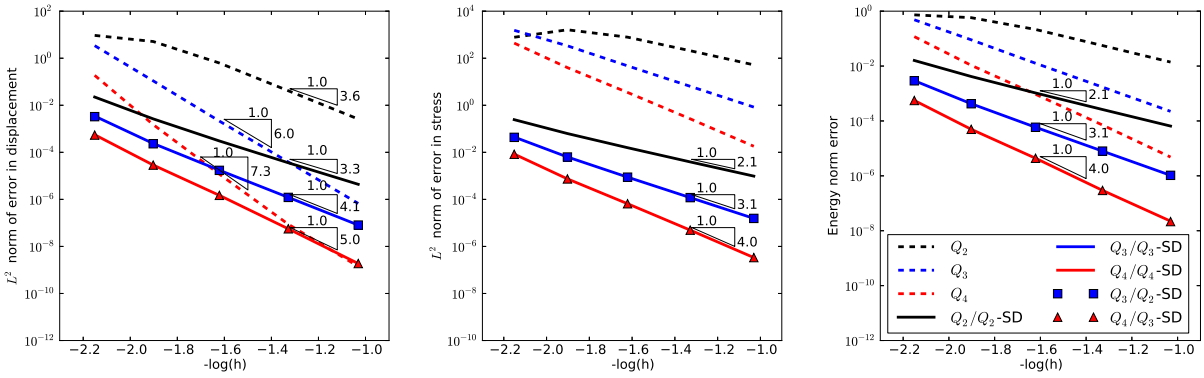

Figure 11: Thick-walled cylinder: error norms for $\nu = 0.49999$.

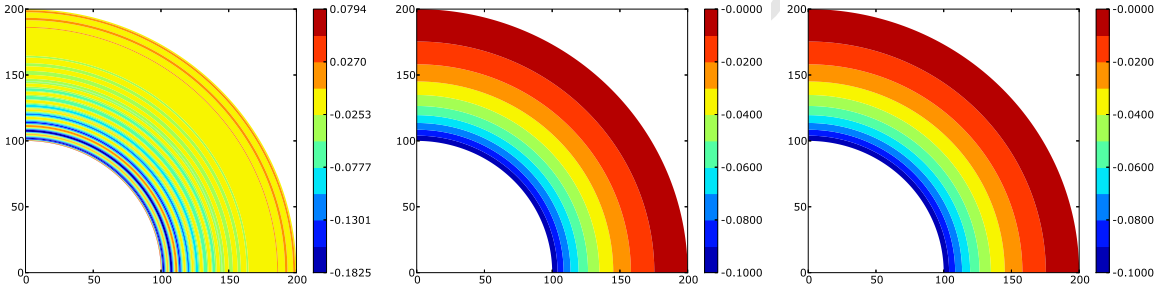

(a) Q_3 (b) Q_3/Q_3-SD (c) Q_3/Q_2-SD

Figure 12: Thick-walled cylinder: contour plots of radial stress (σ_{rr}) with 16×16 mesh with Q_3, Q_3/Q_3-SD and Q_3/Q_2-SD.

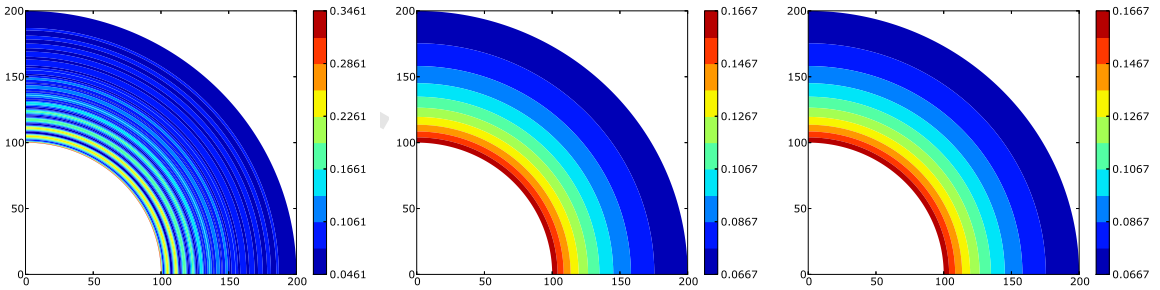

(a) Q_3 (b) Q_3/Q_3-SD (c) Q_3/Q_2-SD

Figure 13: Thick-walled cylinder: contour plots of hoop stress ($\sigma_{\theta\theta}$) with 16×16 mesh with Q_3, Q_3/Q_3-SD and Q_3/Q_2-SD.

6.2. Cook's membrane

Cook's membrane is a standard benchmark problem used to assess the quality of finite element formulation for incompressible solids. In [13, 29, 30] this problem was studied in the context of standard finite element formulations for large strains, while [16, 22, 24, 27, 23] have studied it using NURBS based isogeometric analysis. Geometry, material and boundary conditions of the problem are shown in Fig. 4. The material is assumed to be linear elastic. The value of load, $F = 100$ N/mm is uniformly distributed along the edge of the membrane. Analysis has been performed on successively refined meshes as discussed in 5.4.1, for different orders of NURBS and for different mesh densities for each order, using both the displacement and mixed formulations in order to study their relative performances.

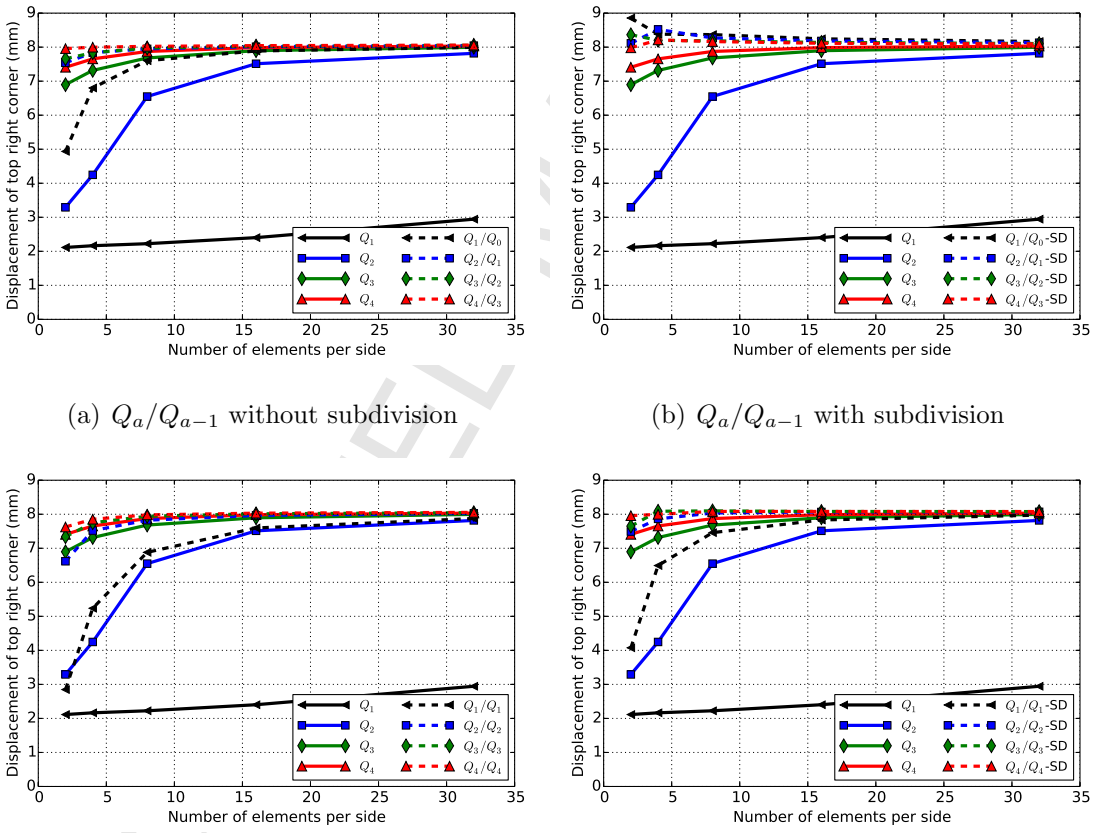

(a) Q_a/Q_{a-1} without subdivision

(b) Q_a/Q_{a-1} with subdivision

(c) Q_a/Q_a without subdivision

(d) Q_a/Q_a with subdivision

Figure 14: Cook's membrane - small strain: vertical displacement of the top right corner versus number of elements per side.

Fig. 14 shows vertical displacement of the top right corner, (point A in Fig. 4), displayed against the number of elements per side for different orders of approximations. As expected, lower order elements with pure displacement formulation suffer from severe locking. Note that even with pure displacement formulation the stiffening effect of locking disappears as the element order is increased. Mixed formulation has clearly helped to improve the accuracy of the result for lower order elements (linear and quadratic), even though it has less significant effect on higher order elements. All of the displacement-pressure combinations studied, with and without subdivision, give improved results over displacement formulation. However, contour plots of hydrostatic pressure, shown in Fig. 15, illustrate that pressure plots obtained with displacement-pressure combinations without subdivision contain spurious oscillations, validating the observations made in Section 5.4.1 by computing the *inf-sup* constants and proves that Q_a/Q_{a-1} NURBS combinations without subdivision are unstable. Based on the results obtained so far we conclude that the combination Q_a/Q_a-SD is the best choice. The remaining examples in this paper are presented with this combination.

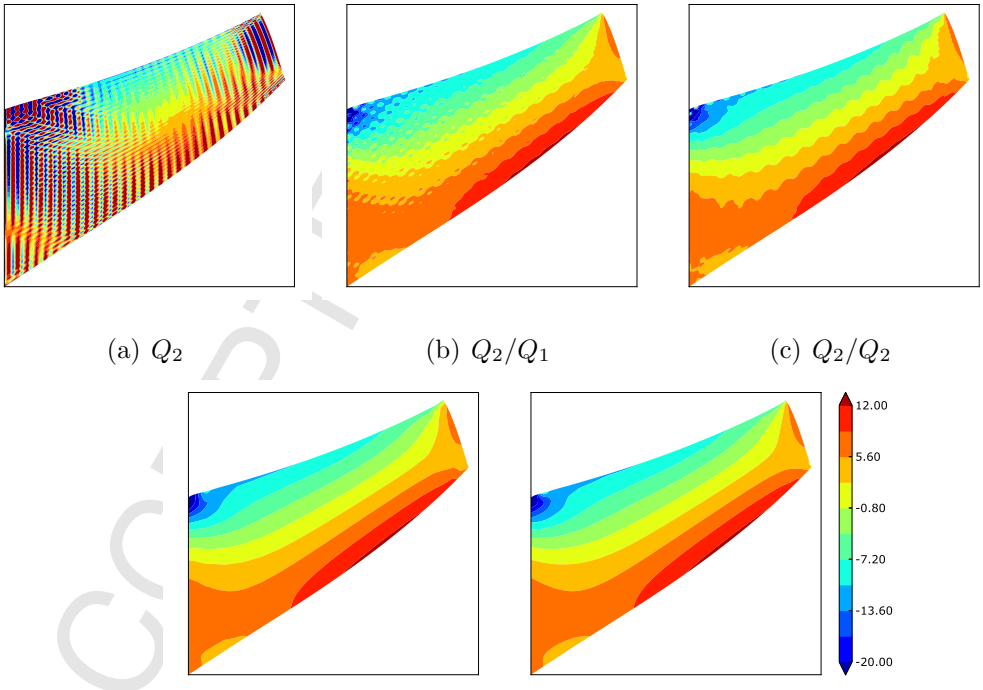

(a) Q_2 (b) Q_2/Q_1 (c) Q_2/Q_2

(d) Q_2/Q_1-SD (e) Q_2/Q_2-SD

Figure 15: Cook's membrane - small strain: hydrostatic pressure for 32x32 mesh with quadratic NURBS.

6.3. Strip footing collapse

This example demonstrates the application of IGA to the determination of the limit load of a strip footing. The problem has been studied by de Souza Neto *et al.* [28] using the standard FEM. The problem consists of a long rectangular footing on top of a soil half-space. The footing is subjected to a vertical pressure, P, and the purpose of the present analysis is to determine the collapse pressure P_{lim}. The soil is assumed to be weightless and is modelled as the von Mises perfectly plastic material. Due to the long length of the footing, the present problem is solved by assuming a plane strain state. Because of the symmetry of the problem geometry and loading, only one half of the cross-section is considered. The geometry, material properties, boundary conditions and loading are shown in Fig. 16(a). The footing is assumed to be rigid and footing/soil interface is assumed to be frictionless. This requires prescribing the vertical displacement u at the control points under the footing and allowing their horizontal displacement to be unconstrained. A total displacement of $u = 0.002$m is applied and the problem is solved by incremental increase of the displacement. The response is measured in terms of the normalized pressure (P/c), where P is total reaction on the footing and the cohesion or shear strength, c, for the von Mises model is given as, $c = \sigma_y/\sqrt{3}$. The results from numerical simulations are compared against the theoretical limit calculated by Prandtl and Hill based on the slip-line theory. For the chosen material properties theoretical limit value is given as $P_{lim} = 5.14\, c$.

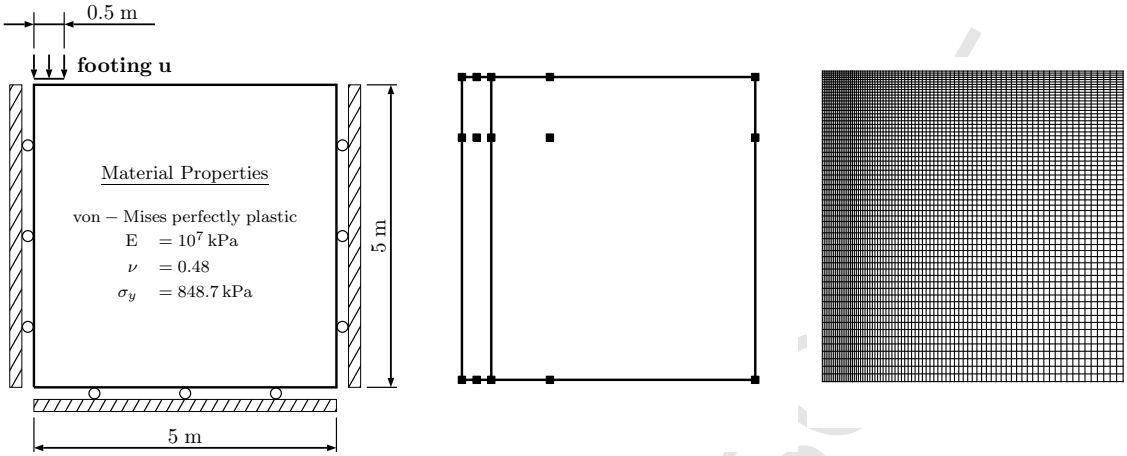

Figure 16: Strip footing collapse: a) geometry, loading, boundary conditions and material properties b) initial control mesh of two patch geometry c) mesh considered for the analysis.

The problem is modelled using two patches so that Dirichlet boundary conditions are applied exactly after refining the mesh using k-refinement. The initial mesh is modelled using quadratic NURBS with a single element in each patch and the initial control points used are as shown in Fig. 16(b). The initial control points are chosen such that the mesh will be suitably refined at the region of interest near the footing and coarse away from it. Analysis is performed on the mesh shown in Fig. 16(c) for different orders of NURBS using both the displacement and mixed formulations.

Fig. 17(a) and Fig. 17(b) show the computed normalized pressure(P/c) against normalized settlement(u/B), respectively, for displacement and mixed formulations and the relative errors in normalized pressure are tabulated in Table.1. Even though the computed collapse loads are within the acceptable limits for both the displacement and mixed formulations, the accuracy of slip line resolution obtained with displacement formulation is very poor as shown in Fig. 18. The use of mixed formulation alleviates this problem and improves the accuracy of slip line resolution as shown in Fig. 19. Contour plots of hydrostatic pressure for both the displacement and mixed formulations shown in Fig. 20. and Fig. 21 indicate again the superior performance of the subdivision based mixed formulation.

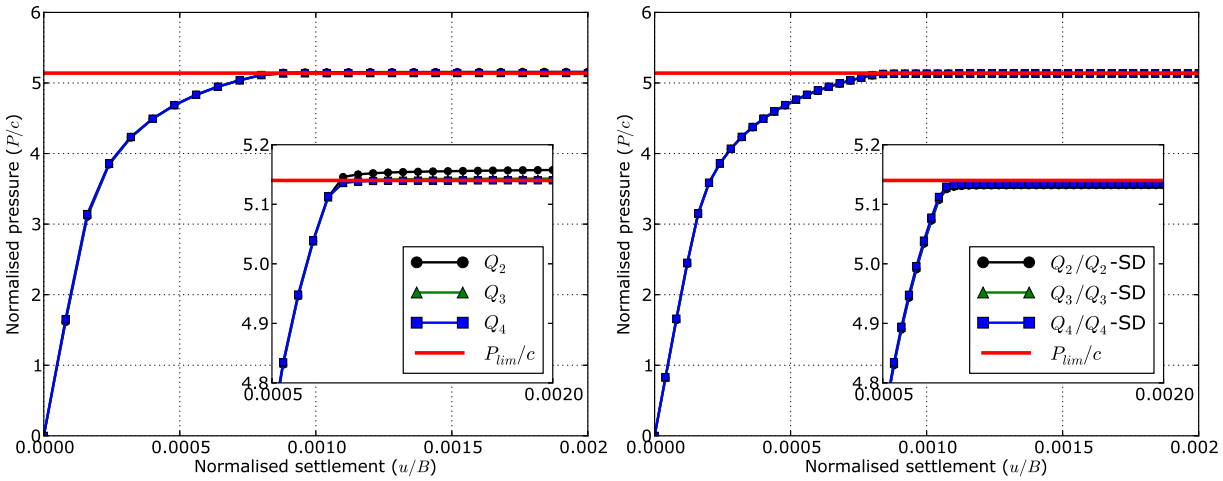

(a) displacement formulation (b) mixed formulation

Figure 17: Strip footing collapse: load-displacement curve.

Degree	disp-formulation	mixed formulation
Q_2	0.3	-0.2
Q_3	0.1	-0.1
Q_4	0.0	-0.1

Table 1: Strip footing collapse: percentage error in normalized pressure.

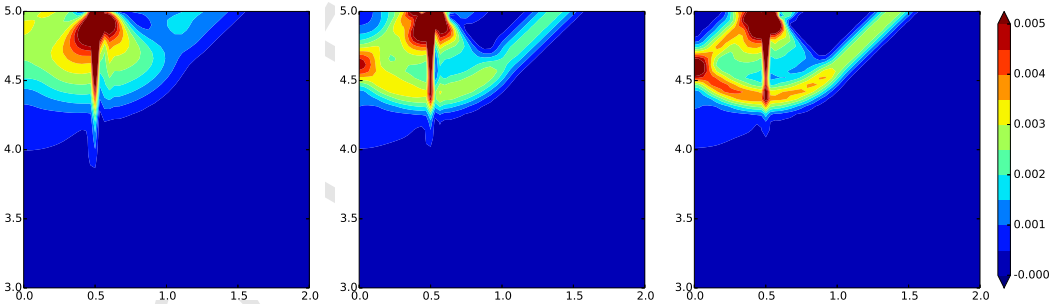

(a) Q_2 (b) Q_3 (c) Q_4

Figure 18: Strip footing collapse: equivalent plastic strain with displacement formulation.

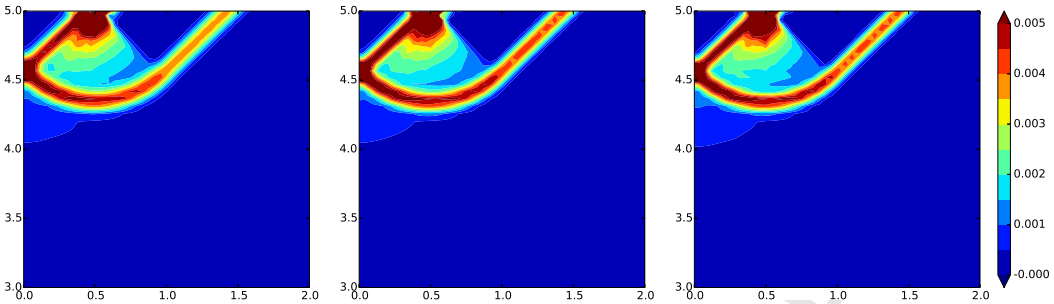

(a) Q_2/Q_2-SD (b) Q_3/Q_3-SD (c) Q_4/Q_4-SD

Figure 19: Strip footing collapse: equivalent plastic strain with mixed formulation.

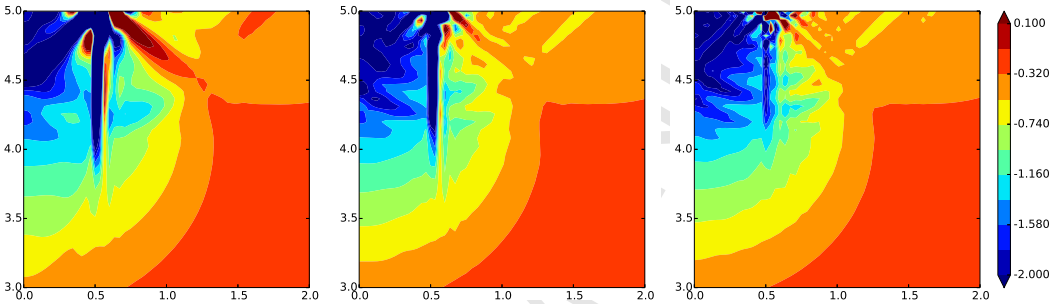

(a) Q_2 (b) Q_3 (c) Q_4

Figure 20: Strip footing collapse: pressure distribution with displacement formulation.

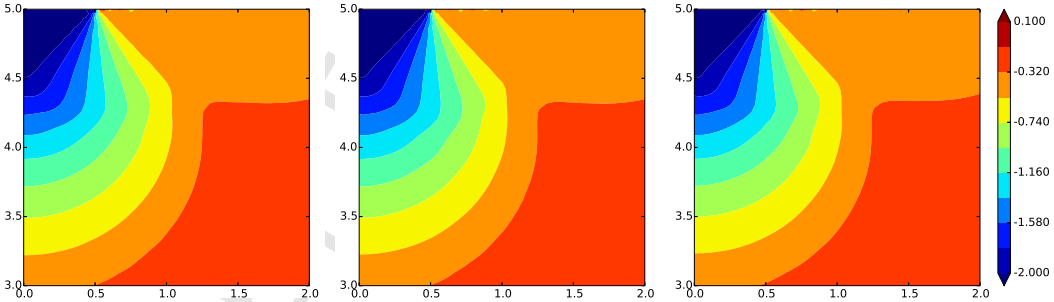

(a) Q_2/Q_2-SD (b) Q_3/Q_3-SD (c) Q_4/Q_4-SD

Figure 21: Strip footing collapse: pressure distribution with mixed formulation.

7. Numerical examples - finite strain

7.1. Cook's membrane with Neo-Hookean hyperelastic material

The geometry, loading and boundary conditions of the problem are same as those used in small strain example. For the purpose of nonlinear analysis the material is modelled using the generalized Neo-Hookean hyperelastic material model in which the stored energy function can be additively decomposed into distortional and volumetric parts, given by,

$$W(J,\bar{\mathbf{b}}) = \frac{1}{2}\mu\left(\mathrm{I}_{\bar{\mathbf{b}}} - 3\right) + \frac{1}{2}\kappa\left(\frac{1}{2}(J^2-1) - \ln J\right) \tag{66}$$

In order to match the material properties in linear range given in Fig. 4, we take, $\kappa = 40.0942 \times 10^4$ MPa and $\mu = 80.1938$MPa. A load value of $F = 100$ N/mm is chosen and it is assumed that the load is conservative, meaning that a fixed load value and direction, equal to that in the reference configuration, is assumed to act during the entire deformation. Similar to small strain formulation, analysis is performed for different discretisations using both the displacement and mixed formulations and the variation of the vertical displacement of the top right corner with respect to number of elements per side is presented in Fig. 22.

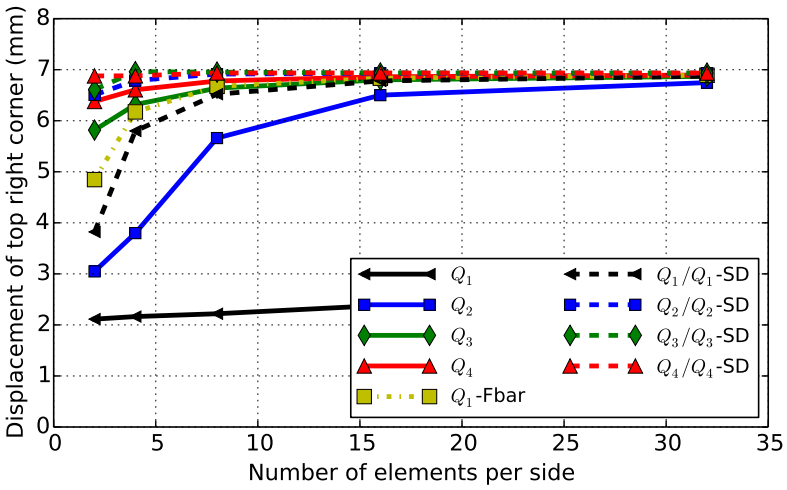

Figure 22: Cook's membrane with Neo-Hookean material: vertical displacement of top right corner versus number of elements per side.

In order to evaluate the performance of the present methods, results obtained with the standard linear quadrilateral element with Fbar formulation of de Souza Neto [29], denoted by Q_1-Fbar, are also presented. Lower order NURBS elements with pure displacement formulation suffer from severe locking problem and accuracy of the results improves with increasing the order of approximation. Mixed formulation substantially improves the accuracy of results as observed in small strain formulation. Higher order NURBS elements with mixed formulation give converged solution even for very coarse meshes.

Table 2 shows the evolution of L_2 norm of residue over different iterations for the last substep of 4x4 mesh with quadratic NURBS for both the formulations. Fig. 23 shows contour plots of hydrostatic pressure for cubic NURBS for 32x32 mesh. Clearly, mixed formulation gives a smooth variation of pressure when compared to the displacement formulation. It is worth noting that as the von Mises equivalent stress is independent of hydrostatic pressure, both formulations give almost identical smooth plots, as shown in Fig. 24.

Iteration number	Norm of residue	
	Displacement formulation	Mixed formulation
1	4.4096 E+00	4.4096 E+00
2	6.1663 E+02	4.4918 E−01
3	5.7846 E−02	2.0436 E−04
4	1.7704 E−02	5.0414 E−11
5	1.1638 E−08	

Table 2: Cook's membrane with Neo-Hookean material: evolution of norm of residual for the last substep for 4x4 mesh with quadratic NURBS.

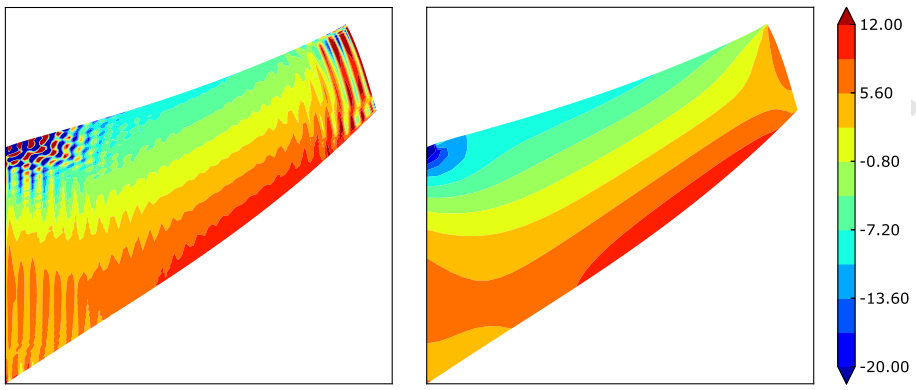

(a) Q_3 (b) Q_3/Q_3-SD

Figure 23: Cook's membrane with Neo-Hookean material: hydrostatic pressure for 32x32 mesh with cubic NURBS.

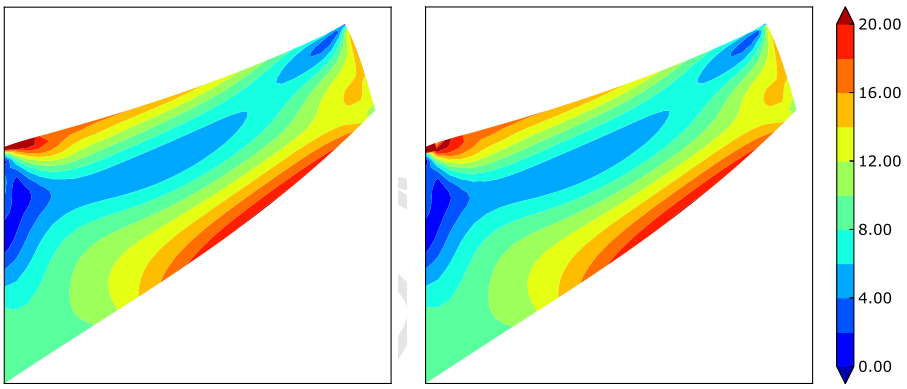

(a) Q_3 (b) Q_3/Q_3-SD

Figure 24: Cook's membrane with Neo-Hookean material: equivalent stress for 32x32 mesh with cubic NURBS.

7.2. Cook's membrane with von Mises elasto-plastic material

In this example, the same Cook's membrane as in previous example is considered but with a different material model and load value. The material model consists of uncoupled stored energy with Neo-Hookean hyperelastic model for the elastic deformations and a plasticity model with associative flow rule based on the von Mises yield criterion with isotropic nonlinear hardening for the plastic portion. Neo-Hookean material model is same as the one

used in the previous example and the nonlinear isotropic hardening law is given by,

$$k(\alpha) = \sigma_0 + (\sigma_\infty - \sigma_0)\left[1 - \exp(-\delta\alpha)\right] + H\alpha, \text{with} \quad \delta > 0 \tag{67}$$

The material properties are: Bulk modulus, $\kappa = 164.21$ GPa, shear modulus, $\mu = 80.1938$ GPa, initial flow stress, $\sigma_0 = 450$ MPa, saturation flow stress, $\sigma_\infty = 715$ MPa, saturation exponent, $\delta = 16.93$ and linear hardening coefficient, $H = 129.24$ MPa.

A load value of $F = 20$ kN/mm is used. Similar to the previous example, analysis is performed for different orders of approximations for all five meshes using both displacement and mixed formulations and a similar pattern in the convergence of results is observed. Variation of the displacement of top right corner against the number of elements per side, for different orders of approximations, is shown in Fig. 25. Clearly, mixed formulation substantially improves the accuracy of the results. Figs. 26 and 27 show the contour plots of equivalent plastic strain and von Mises equivalent stress, respectively, for cubic NURBS for both displacement and mixed formulations.

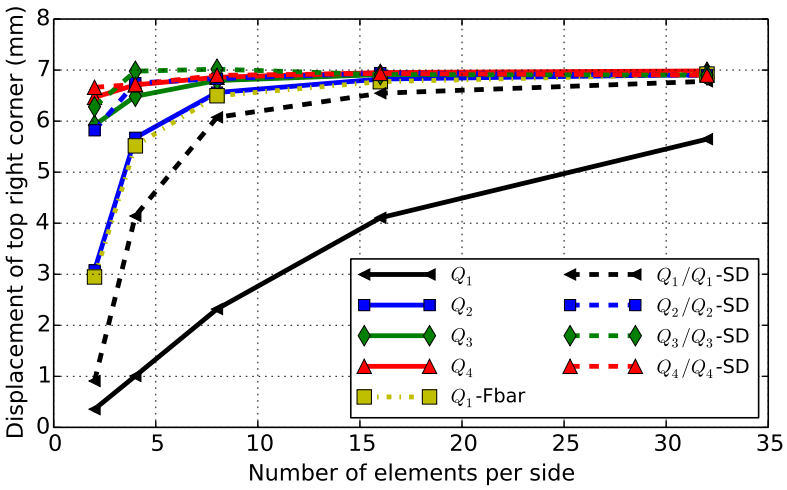

Figure 25: Cook's membrane with elasto-plastic material: vertical displacement of top right corner versus number of elements per side.

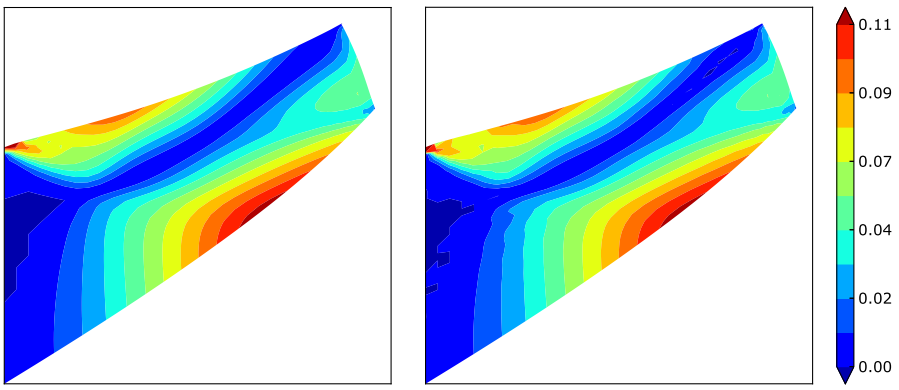

(a) Q_3 (b) Q_3/Q_3-SD

Figure 26: Cook's membrane with elasto-plastic material: equivalent plastic strain for 32x32 mesh with cubic NURBS.

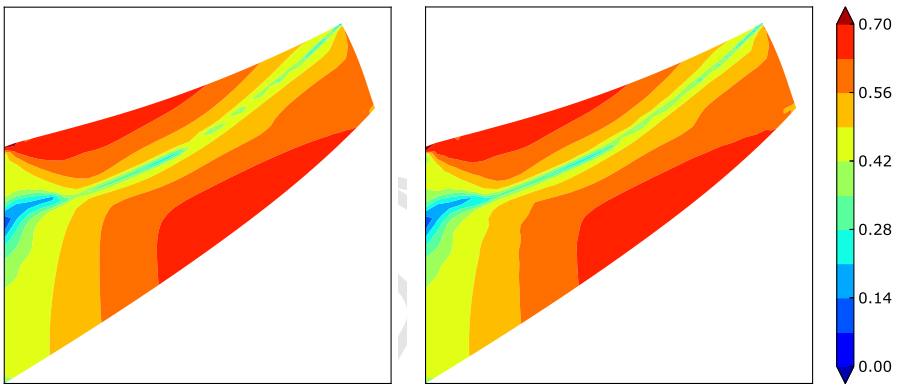

(a) Q_3 (b) Q_3/Q_3-SD

Figure 27: Cook's membrane with elasto-plastic material: equivalent stress for 32x32 mesh with cubic NURBS.

7.3. Plane strain compression of a block

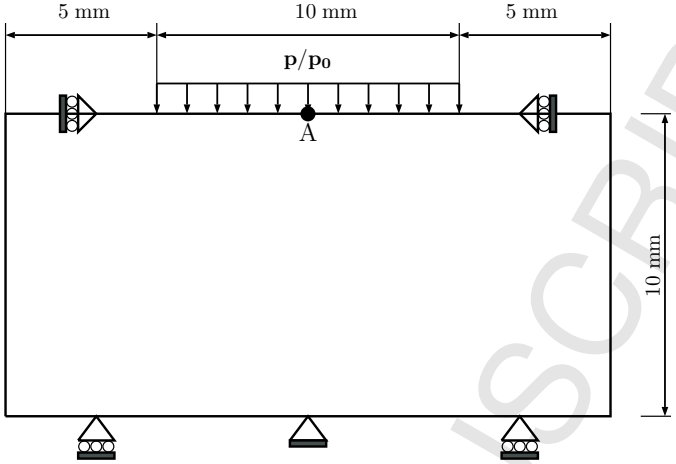

Figure 28: Block under compression: Geometry, loading and boundary conditions.

This problem has been studied by Reese *et al.* [33] and since then has been used as a standard benchmark problem to study the performance of various finite element formulations to deal with incompressibility in finite strains. Elguedj *et al.* [16] and Kadapa *et al.* [22, 24] studied this problem in the context of isogeometric analysis. This problem consists of a block resting on a rigid surface and subjected to pressure loading at its middle portion. The geometry, boundary conditions and loading are as shown in Fig. 28. Due to the symmetry of geometry, boundary and loading conditions, only half of the model is considered for the analysis. The material is modelled using Neo-Hookean material model with the following strain energy function,

$$W(J,\bar{\mathbf{b}}) = \frac{1}{2}\mu\left(\mathrm{I}_{\bar{\mathbf{b}}} - 3\right) + \frac{1}{4}\lambda\left((J^2-1) - 2\ln J\right) - \mu \ln J \tag{68}$$

with material parameters $\lambda = 400889.806$ MPa and $\mu = 80.1938$ MPa. The load is assumed to be conservative. The quantity of interest is the compression level (vertical displacement) of top middle, point A in Fig. 28. Variation of compression level is studied for different loading conditions, i.e. different p/p_0 values with $p_0 = 20$, for different orders of NURBS approximation spaces using the proposed mixed formulation. Results obtained for Q_1/Q_1-SD NURBS are compared with those obtained using the standard 4-node linear-quadrilateral

element of FEM with Fbar formulation, denoted as Q_1-Fbar, (see de Souza Neto *et al.* [29]). Convergence is obtained, for all the considered loading conditions, with a mesh of 16x16 and is shown in Fig. 29. Fig. 30 shows the variation of compression level for different loading conditions, p/p_0=20, 40, 60, using both the displacement and mixed formulations for different orders of NURBS spaces. Again, convergence is obtained with 16x16 meshes, except for Q_1 NURBS. Q_1 NURBS for all the meshes and Q_2 NURBS for coarse meshes suffer from sever locking problems and increasing the order of NURBS improves the accuracy. Similar to the Cook's membrane response, mixed formulation substantially improves the accuracy even for coarse meshes and improvement in accuracy, with mixed formulation, becomes negligible for higher order NURBS with fine meshes. However, it has been observed that mixed formulation converges with substantially less number of load steps compared to the pure displacement formulation. Therefore, use of mixed formulation reduces the overall computational time and also gives more accurate results and smooth variation of stresses. Figs. 31 and 32 show, respectively, the contour plots of hydrostatic pressure and von Mises equivalent stress, for 32x32 mesh with cubic NURBS for p/p_0=60.

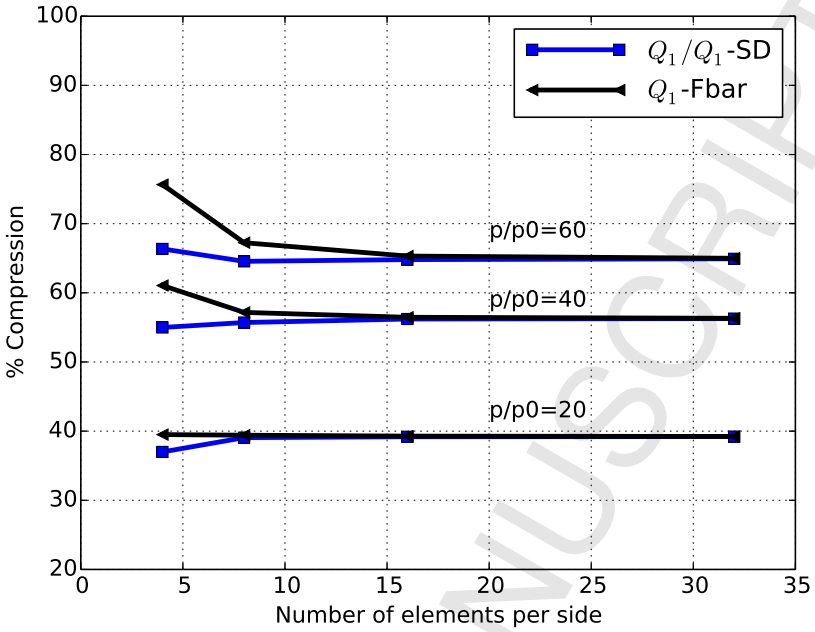

Figure 29: Block under compression: compression level for Q_1/Q_0 NURBS compared to Linear-Quadrilateral(LQ) element in standard FEM with Fbar formulation of de Souza Neto *et. al.* [29].

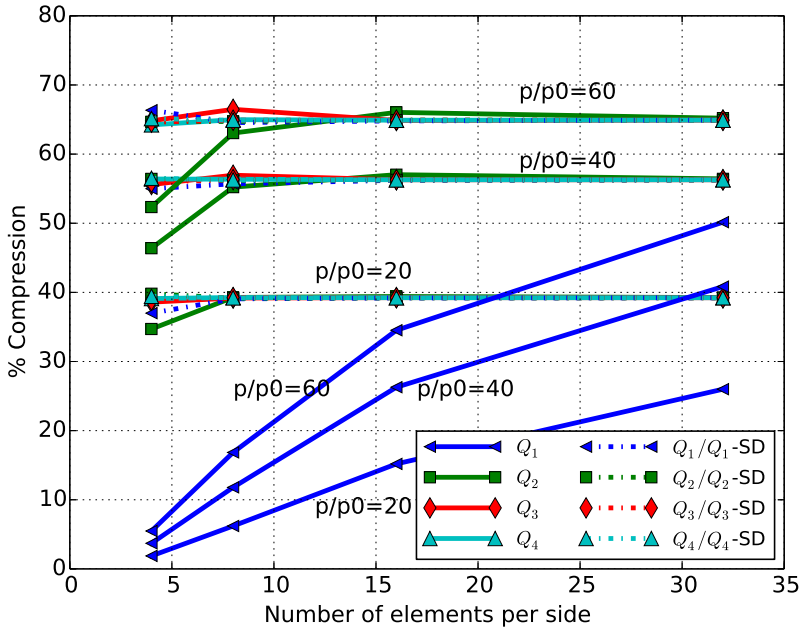

Figure 30: Block under compression: compression level for different orders of NURBS under different loading conditions.

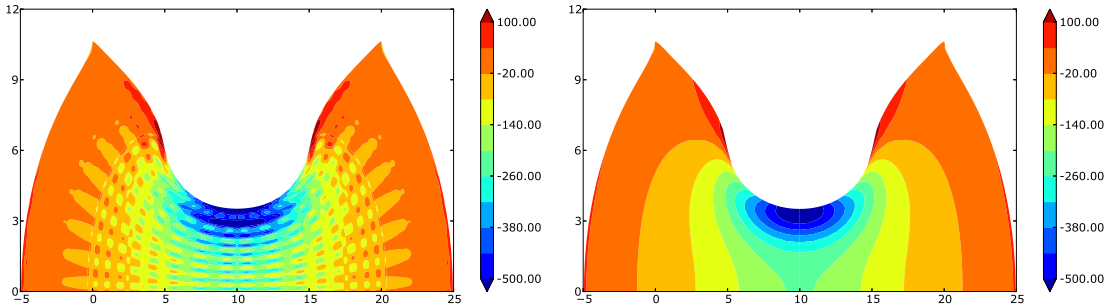

(a) Q_3 (b) Q_3/Q_3-SD

Figure 31: Block under compression: contour plots of hydrostatic pressure for 32x32 mesh with cubic NURBS with p/p_0=60.

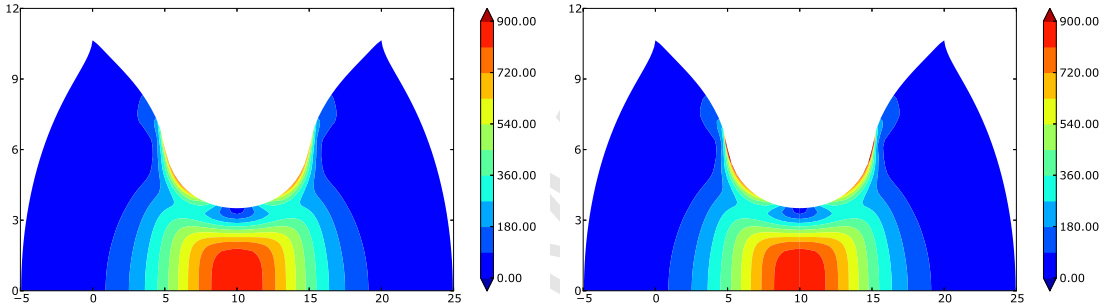

(a) Q_3 (b) Q_3/Q_3-SD

Figure 32: Block under compression: contour plots of Von-Mises equivalent stress for 32x32 mesh with cubic NURBS with p/p_0=60.

7.4. Necking of an elasto-plastic strip

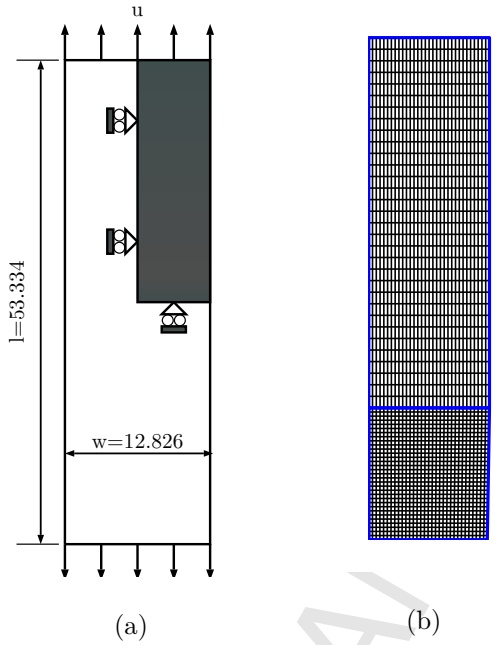

Figure 33: Necking of an elasto-plastic strip: a) geometry, loading and boundary conditions and b) mesh used for the analysis. Blue lines indicate patch boundaries.

In this example we study the plane strain localization of a strip subjected to uniform extension. This problem has been studied by several authors [4, 27, 29, 30, 40, 44] and is considered as standard benchmark problem for testing the behaviour of finite element formulations for incompressible plastic materials at finite strains. The geometry and loading conditions are as shown in Fig. 33. The material model and material properties are same as those used in Cook's membrane with finite strain plasticity. Due to obvious symmetry only quarter portion of the model is considered for the analysis. In order to trigger strain localization, a width reduction of 1.8% is introduced in the center of the bar. A total vertical displacement of $u = 5.0$ is applied on the top edge and the problem is solved in several load steps. Figs. 34(a) and 34(b) show the plots of variation of necking displacement and necking force, respectively, with respect to the variation of applied displacement for different orders of NURBS spaces.

Contour plots of stress component (σ_{yy}), pressure (p) and equivalent plastic strain (α)

are shown in Fig. 35 and Fig. 36, for linear and quadratic NURBS, respectively. The mixed formulation with the proposed displacement-pressure combination improves the quality of results substantially for linear elements and the improvement for quadratic NURBS is not so pronounced as the results obtained by displacement formulation are already of good quality.

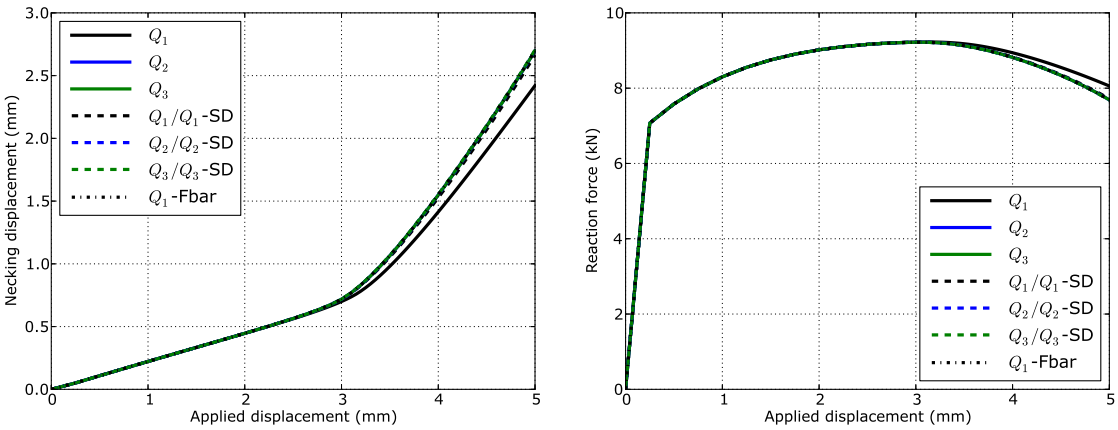

(a) Necking displacement (b) Reaction force

Figure 34: Necking of an elasto-plastic strip: necking displacement and reaction force versus applied displacement.

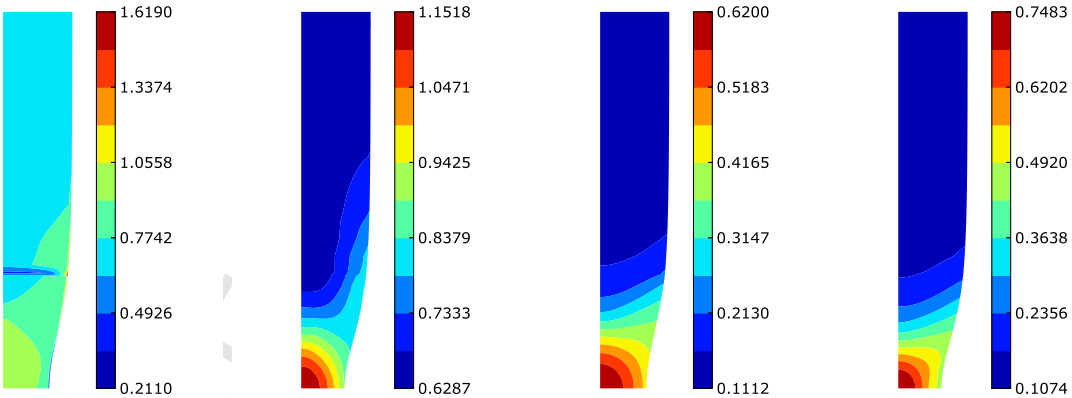

(a) σ_{yy} with Q_1 (b) σ_{yy} with Q_1/Q_1-SD (c) α with Q_1 (d) α with Q_1/Q_1-SD

Figure 35: Necking of an elasto-plastic strip: contour plots with linear NURBS: (a)-(b) σ_{yy} stress and (c)-(d) equivalent plastic strain (α).

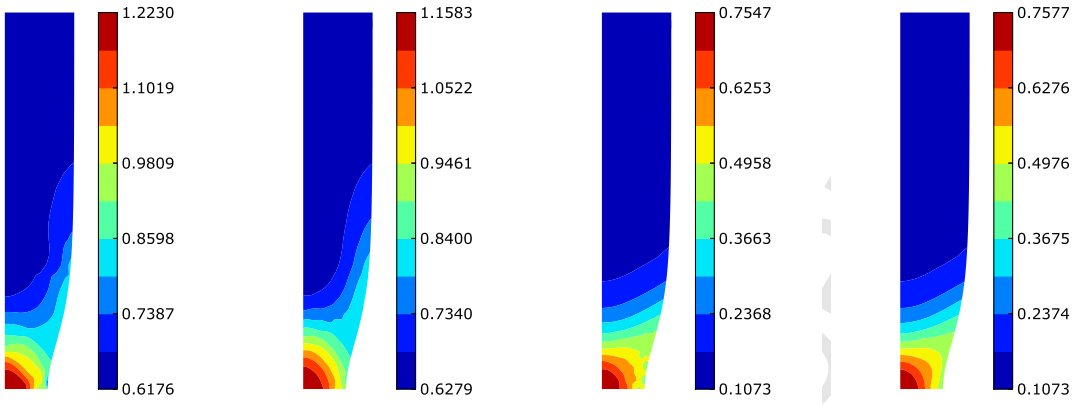

(a) σ_{yy} with Q_2 (b) σ_{yy} with Q_2/Q_2-SD (c) α with Q_2 (d) α with Q_2/Q_2-SD

Figure 36: Necking of an elasto-plastic strip: contour plots with quadratic NURBS: (a)-(b) σ_{yy} stress and (c)-(d) equivalent plastic strain (α).

7.5. Torsion of a square prism

In this example we present the performance of mixed methods under severe mesh distortions, using the torsion of a square prism. This problem was studied by Lipton *et al.* [26] using $\bar{\mathbf{F}}$ formulation with NURBS and Kadapa *et al.* [22, 24] using mixed formulation. Geometry and boundary conditions of the problem are as shown in Fig. 37(a). Rotation (θ_z) on the top face is applied in the form of X and Y directional displacements. Material model and material properties are same as those used in Cook's membrane with Neo-Hookean hyperelastic material. A 4x4x16 mesh is studied with subdivision stabilised displacement-pressure combinations with linear, quadratic and cubic NURBS.

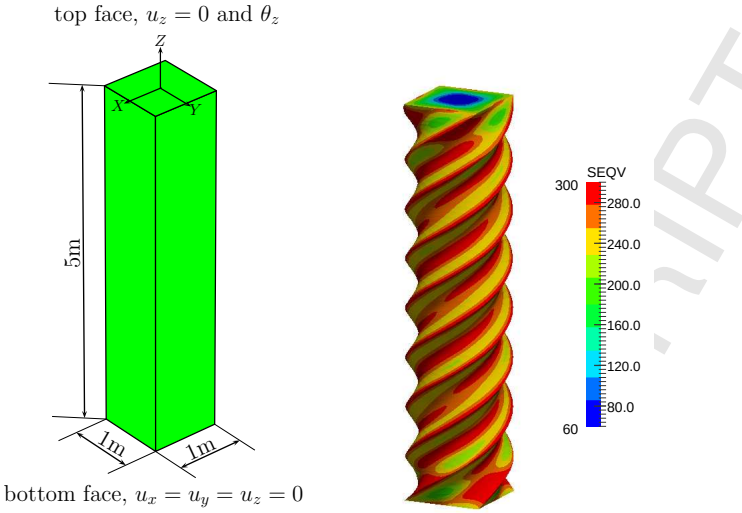

(a) (b)

Figure 37: Torsion of a prism: a) geometry, loading and boundary conditions, and b) von Mises stress contour plot at 720 deg rotation for Q_2/Q_2-SD.

The quantity of interest in the present example is the maximum angle of twist that a mesh can sustain before failing to converge. Failure angles for the different discretisations considered in the study are presented in Table. 3. Analyses performed with mixed formulation have shown exceptional reduction in computational time when compared with the displacement formulation. Mixed formulation converges with increments of 10 deg while displacement formulation needs an increment of 1 deg and sometimes even less. On average, 10-fold reduction in computational time is achieved using mixed formulation. This reduction in computational time proves to be extremely beneficial in large-scale engineering simulations. A typical deformed shape of the bar along with von Mises stress distribution for an intermediate configuration (at $\theta = 720$ deg) is shown in Fig. 37(b).

Table 3: Torsion of a prism: failure angle in degrees.

NURBS basis	Failure angle for Q_a/Q_a-SD
Linear (Q_1)	**890**
Quadratic (Q_2)	**830**
Cubic (Q_3)	**990**

7.6. Bending of a thick cylindrical shell

This example is used to demonstrate the performance of the finite element formulations to deal with the issue of "shear locking" of shells. This problem was studied by [10, 13, 34]. The geometry, loading and material properties are as shown in Fig. 38. As the Poisson's ratio is only 0.4 no volumetric locking is expected; however, because of the geometry, this problem suffers from shear locking. Due to symmetry of geometry and loading conditions, only a 1/8th portion is considered for the analysis, as shown in Fig. 39(a), along with boundary conditions and loading and a typical mesh used. Due to circular cross sections the initial geometry has to be modelled with quadratic NURBS. The load is assumed to be conservative and a Neo-Hookean material model with the following energy function is used,

$$\Psi(J,\bar{\mathbf{C}}) = \frac{1}{2}\mu\left(\mathrm{tr}[\bar{\mathbf{C}}]-3\right) - \mu\ln J + \frac{1}{2}\lambda\left(\ln J\right)^2 \tag{69}$$

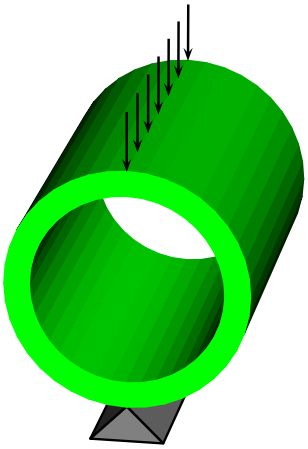

Total length	L	$= 30$ mm
Inner radius	R_i	$= 8$ mm
Outer radius	R_o	$= 10$ mm
Young′s modulus	E	$= 16800$ MPa
Poisson′s ratio	ν	$= 0.4$
Applied load	p	$= 450$ N/mm

Figure 38: Bending of a thick cylindrical shell: geometry, loading and material properties.

While only one element is considered in the thickness direction in [10, 13, 34] we consider two elements in the thickness direction in order to use the proposed subdivision-stabilised displacement-pressure combination. Meshes with densities 2x4x2, 4x8x2, 8x16x2 and 16x32x2, are analysed with linear, quadratic and cubic NURBS using both the displacement and mixed formulations. The 2x4x2 mesh implies that there are 2 elements in axial direction, 4 elements in circumferential direction and 2 element through the thickness.

The quantity of interest is the vertical displacement of point A shown in Fig. 39(a). Variation of the vertical displacement at point A, for different discretisations, as shown in Fig. 40 illustrates the convergence pattern. It is worth mentioning that displacement formulation suffers to converge with the large load increments for this problem also while the mixed formulation converges in only 5 load increments. The deformed shape along with the contour plot of σ_{yy} stress for 16x32x2 mesh with Q_2/Q_2-SD is shown in Fig. 41.

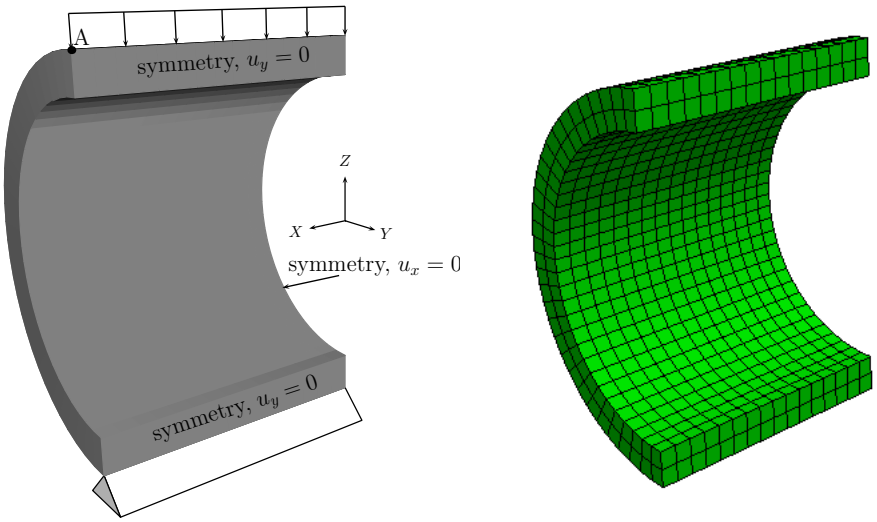

(a) Boundary conditions (b) 16x32x2 mesh

Figure 39: Bending of a thick cylindrical shell: boundary conditions and a typical mesh used for the analysis.

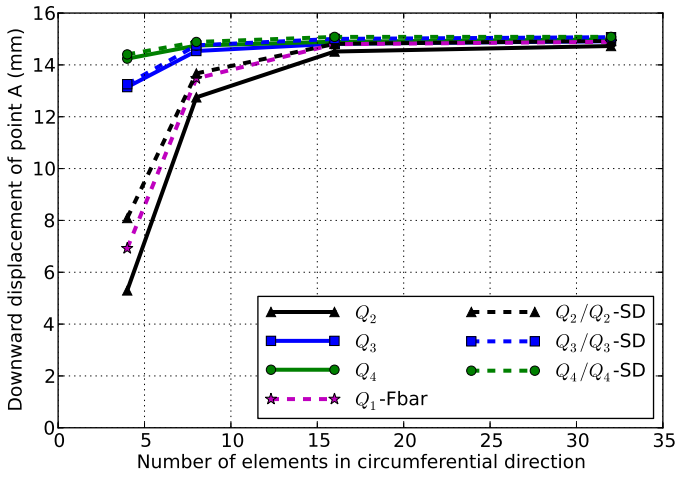

Figure 40: Bending of a thick cylindrical shell: downward displacement of point A with respect to number of elements in the circumferential direction for different order of NURBS with displacement and mixed formulation.

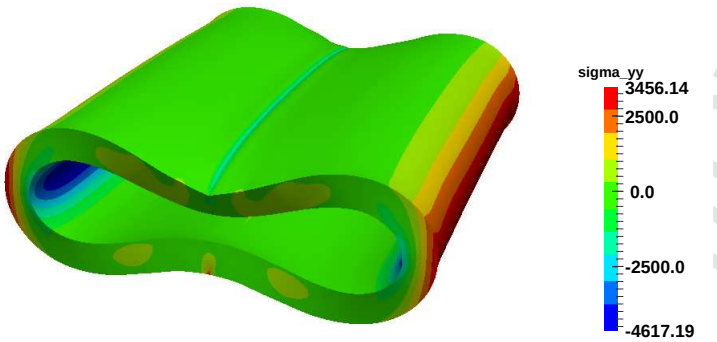

Figure 41: Bending of a thick cylindrical shell: contour plot of σ_{yy} stress.

8. Summary and conclusions

In this work we have presented robust two-field mixed variational formulations for both small and finite strain problems to deal with the issues of incompressibility in the context of NURBS based isogeometric analysis. *Inf-sup* stable displacement-pressure combinations are developed based on the subdivision properties of NURBS. The *inf-sup* stability of proposed displacement-pressure combinations is demonstrated by computing the numerical *inf-sup* constants for Cook's membrane and thick-walled cylinder. The convergence of the proposed discretisations is demonstrated, numerically, for linear elastic thick-walled cylinder. Some important features of the present work can be summarised as:

- The formulations are straightforward two-field mixed Galerkin formulations. They are simple, elegant and easy to implement.
- Higher-order NURBS basis with higher continuities across element boundaries are used for both the displacement and pressure discretisations thereby preserving the salient feature of NURBS based isogeometric analysis.
- The formulations do not involve any element-level or patch-level matrix inversions.
- Optimal convergence rates are obtained for the linear problems.
- The solution can be obtained with large load increments.

Performance of the proposed formulations is demonstrated by studying a wide range of benchmark problems. Numerical results show that higher order NURBS with mixed formulations perform excellently even for coarse meshes. The robustness of the proposed method for problems involving severe mesh deformations is demonstrated on the torsion of square prism. Moreover, the results obtained in the present work clearly show that two-field mixed formulations are sufficient enough to obtain accurate numerical solutions for all the material models considered without any need to employ the three-field mixed formulations.

All the examples studied in the present work are based on full tensor-product meshes generated with NURBS. The main disadvantage of the tensor-product meshes is that they lack local refinement capability because of which the domain has to be refined globally. This global refinement results in unnecessary DOF far away from the zone of interest, as observed in *strip footing collapse* example, thereby increasing the total size of the system. Hence, in order to increase the efficiency of the mixed formulations studied in the work, we suggest extending the proposed formulations to the local refinement schemes [39, 46].

References

[1] PARDISO solver project. (http://www.pardiso-project.org).

[2] C. Adam, and T. J. R. Hughes, and S. Bouabdallah, and M. Zarroug, and H. Maitournam. Selective and reduced numerical integrations for NURBS-based isogeometric analysis. Computer Methods in Applied Mechanics and Engineering, 284:732-761, 2015.

[3] P. Antolin, and A. Buffa, and G. Sangalli. An isogeometric method for quasi-incompressible elasticity with local stress projection. 3rd international conference on isogeometric analysis, IGA 2015, Trondheim, Norway, 2015.

[4] F. Armero and S. Glaser. On the formulation of enhanced strain finite elements in finite deformations. *Engineering Computations*, 14:759–791, 1997.

[5] Y. Bazilevs, V. M. Calo, T. J. R. Hughes, and Y. Zhang. Isogeometric fluid-structure interaction: theory, algorithms, and computations. *Computational Mechanics*, 43:3–37, 2008.

[6] J. Bonet, and R. D. Wood. Nonlinear continuum mechanics for finite element analysis. Cambridge University Press, USA, 1997.

[7] A. Bressan, and G. Sangalli. Isogeometric discretizations of the Stokes problem: stability analysis by the macroelement technique. *IMA Journal of Numerical Analysis*, 33:629–651, 2013.

[8] F. Brezzi and R. S. Falk. Stability of higher-order Hood-Taylor methods. *SIAM Journal on Numerical Analysis*, 28:581–590, 1991.

[9] F. Brezzi and M. Fortin. *Mixed and Hybrid Finite Element Methods*. Springer-Verlag, 1991.

[10] N. Büchter, E. Ramm, and D. Roehl. Three-dimensional extension of non-linear shell formulation based on the enhanced assumed strain concept. *International Journal for Numerical Methods in Engineering*, 37:2551–2568, 1994.

[11] A. Buffa, C. de Falco, and G. Sangalli. Isogeometric analysis: stable elements for the 2D Stokes equation. *International Journal for Numerical Methods in Fluids*, 65:1407–1422, 2011.

[12] D. Chapelle and K. J. Bathe. The inf-sup test. *Computers and Structures*, 47:537–545, 1993.

[13] K. S. Chavan, B. P. Lamichhane, and B. I. Wohlmuth. Locking-free finite element methods for linear and nonlinear elasticity in 2D and 3D. *Computer Methods in Applied Mechanics and Engineering*, 196:4075–4086, 2007.

[14] J. A. Cottrell, Y. Bazilevs, and T. J. R. Hughes. *Isogeometric analysis: toward integration of CAD and FEA*. John Wiley & Sons, Chichester, England, 2009.

[15] J. A. Cottrell, A. Reali, Y. Bazilevs, and T. J. R. Hughes. Isogeometric analysis of structural vibrations. *Computer Methods in Applied Mechanics and Engineering*, 195:5257–5296, 2006.

[16] T. Elguedj, Y. Bazilevs, V.M. Calo, and T. J. R. Hughes. $\bar{\mathrm{B}}$ and $\bar{\mathrm{F}}$ projection methods for nearly incompressible linear and non-linear elasticity and plasticity using higher-order NURBS elements. *Computer Methods in Applied Mechanics and Engineering*, 197:2732–2762, 2008.

[17] T. Elguedj and T. J. R. Hughes. Isogeometric analysis of nearly incompressible large strain plasticity. *Computational Methods in Applied Mechanics and Engineering*, 268:388–416, 2014.

[18] G. Farin. *Curves and Surfaces for CAGD, A practical guide*. Academic Press, San Diego, CA, first edition, 2002.

[19] H. Gomez, T. J. R. Hughes, X. Nogueira, and V. M. Calo. Isogeometric analysis of the isothermal Navier-Stokes-Korteweg equations. *Computer Methods in Applied Mechanics and Engineering*, 199:1828–1840, 2010.

[20] T. J. R. Hughes. *The Finite Element Method: Linear Static and Dynamic Finite Element Analysis*. Dover Publications, New York, 2000.

[21] T. J. R. Hughes, Y. Bazilevs, and J. A. Cottrell. Isogeometric analysis: CAD, finite elements, NURBS, exact geometry and mesh refinement. *Computer Methods in Applied Mechanics and Engineering*, 194:4135–4195, 2005.

[22] C. Kadapa. *Mixed Galerkin and least-squares formulations for isogeometric analysis*. PhD thesis, 2014.

[23] C. Kadapa, W. G. Dettmer, and D. Perić. NURBS based least-squares finite element methods for fluid and solid mechanics. *International Journal for Numerical Methods in Engineering*, 101:521–539, 2015.

[24] C. Kadapa, W. G. Dettmer, and D. Perić. Mixed methods for isogeometric analysis of nearly incompressible materials. In *XII International conference on Computational Plasticity. Fundamentals and Applications, Barcelona, Spain, September 2013.*, 2013.

[25] C. Kadapa, W. G. Dettmer, and D. Perić. Inf-sup stable displacement-pressure combinations for isogeometric analysis of nearly incompressible materials. 3rd international conference on isogeometric analysis, IGA 2015, Trondheim, Norway, 2015.

[26] S. Lipton, J. A. Evans, Y. Bazilevs, T. Elguedj, and T. J. R. Hughes. Robustness of isogeometric structural discretizations under severe mesh distortion. *Computer Methods in Applied Mechanics and Engineering*, 199:357–373, 2010.

[27] K. M. Mathisen, K. M. Okstad, T. Kvamsdal, and S. B. Raknes. Isogeometric analysis of finite deformation nearly incompressible solids. *Journal of Structural Mechanics*, 44(3):260–278, 2011.

[28] E. A. de Souza Neto, D. Perić, and D. R. J. Owen. *Computational Methods for Plasticity, Theory and Applications*. John Wiley and Sons, United Kingdom, 2008.

[29] E. A. de Souza Neto, D. Perić, M. Dutko, and D. R. J. Owen. Design of simple low order finite elements for large strain analysis of nearly incompressible solids. *International Journal of Solids Structures*, 33:3277–3296, 1996.

[30] E. A. de Souza Neto, F. M. A. Pires, and D. R. J. Owen. F-bar-based linear triangles and tetrahedra for finite strain analysis of nearly incompressible solids. Part I: formulation and benchmarking. *International Journal for Numerical Methods in Engineering*, 62:353–383, 2005.

[31] T. H. H. Pian and C. C. Wu. *Hybrid and Incompatible Finite Element Methods*. Chapman and Hall/CRC, 2006.

[32] L. Piegl and W. Tiller. *The NURBS Book (Monographs in Visual Communication)*. Springer-Verlag, New York, 1997.

[33] S. Reese, M. Kussner, and B. D. Reddy. A new stabilization technique for finite elements in non-linear elasticity. *International Journal for Numerical Methods in Engineering*, 44:1617–1652, 1999.

[34] S. Reese, P. Wriggers, and B. D. Reddy. A new locking-free brick element technique for large deformation problems in elasticity. *Computers and Structures*, 75:291–304, 2000.

[35] D. F. Rogers. *An Introduction to NURBS With Historical Perspective*. Academic Press, San Diego, CA, 2001.

[36] T. Rüberg and F. Cirak. Subdivision-stabilised immersed b-spline finite elements for moving boundary flows. *Computer Methods in Applied Mechanics and Engineering*, 209-212:266–283, 2012.

[37] T. Rüberg and F. Cirak. A fixed-grid b-spline finite element technique for fluid-structure interaction. *International Journal for Numerical Methods in Fluids*, 74:623–660, 2014.

[38] G. Sangalli. Isogeometric analysis for nearly incompressible materials. London Mathematical Society

EPSRC Durham Symposium. Building bridges: connections and challenges in modern approaches to numerical partial differential equations, 2014.

[39] D. Schillinger, L. Dedè, M. A. Scott, J. A. Evans, M. J. Borden, E. Rank, and T. J. R. Hughes. An isogeometric design-through-analysis methodology based on adaptive hierarchical refinement of NURBS, immersed boundary methods, and T-spline CAD surfaces. *Computer Methods in Applied Mechanics and Engineering*, 249-252:116–150, 2012.

[40] J. C. Simo and F. Armero. Geometrically non-linear enhanced strain mixed methods and the method of incompatible modes. *International Journal for Numerical Methods in Engineering*, 33:1413–1449, 1992.

[41] J. C. Simo and T. J. R. Hughes. On the variational foundations of assumed strain methods. *Journal of Applied Mechanics*, 53:51–54, 1986.

[42] J. C. Simo and T. J. R. Hughes. *Computational Inelasticity*, volume 7 of *Interdisciplinary Applied Mathematics*. Springer, Berlin, Germany, 1998.

[43] J. C. Simo and M. S. Rifai. A class of mixed assumed strain methods and the method of incompatible modes. *International Journal for Numerical Methods in Engineering*, 29:1595–1638, 1990.

[44] R. L. Taylor. Isogeometric analysis of nearly incompressible solids. *International Journal for Numerical Methods in Engineering*, 87:273–288, 2011.

[45] S. P. Timoshenko and J. N. Goodier. *Theory of Elasticity*. McGraw-Hill, third ed., New York, 1970.

[46] A.-V. Vuong, C. Giannelli, B. Jüttler, and B. Simeon. A hierarchical approach to adaptive local refinement in isogeometric analysis. *Computer Methods in Applied Mechanics and Engineering*, 200:3554–3567, 2011.

[47] O. C. Zienkiewicz and R. L. Taylor. *The Finite Element Method for Solid and Structural Mechanics*, sixth edition, Elsevier Butterworth and Heinemann, Oxford, England, 2005.